Copy
RM L54L23

NACA RM L54L23

NACA

# RESEARCH MEMORANDUM

## DEVELOPMENT OF A NEW FLUTTER TESTING TECHNIQUE USING A TOWED DYNAMIC AIRPLANE MODEL EQUIPPED WITH AN AUTOMATIC STABILIZING SYSTEM

## EXPERIMENTAL AND CALCULATED DYNAMIC STABILITY CHARACTERISTICS FOR SPEEDS UP TO 200 MPH

By William C. Schneider

Langley Aeronautical Laboratory
Langley Field, Va.

NATIONAL ADVISORY COMMITTEE
FOR AERONAUTICS

WASHINGTON
March 25, 1955
Declassified January 10, 1957

NACA RM L54L23

NATIONAL ADVISORY COMMITTEE FOR AERONAUTICS

RESEARCH MEMORANDUM

# DEVELOPMENT OF A NEW FLUTTER TESTING TECHNIQUE USING A TOWED DYNAMIC AIRPLANE MODEL EQUIPPED WITH AN AUTOMATIC STABILIZING SYSTEM

## EXPERIMENTAL AND CALCULATED DYNAMIC STABILITY CHARACTERISTICS FOR SPEEDS UP TO 200 MPH

By William C. Schneider

## SUMMARY

Tests of a towed airplane model have been made in the Langley 19-foot pressure tunnel in conjunction with the development of a flutter testing technique. The model was equipped with a suitable autopilot to keep the model flying straight and level in the tunnel while restrained only in drag. Flights were made through the speed range of the tunnel up to a maximum speed of 200 mph at atmospheric pressure with both rigid and flexible wings.

The dynamic stability of the model-autopilot-towline combination was investigated analytically and an attempt was made to correlate the results with experiment. Only qualitative comparison with flight impressions was possible due to a random tunnel airstream disturbance of unknown origin.

## INTRODUCTION

Tests in the Langley 19-foot pressure tunnel of a towed airplane model have recently been completed in conjunction with the development of a testing technique which allows body freedoms during flutter tests (ref. 1). The model was flown on the end of a tow cable attached to the nose of the model. Suitable autopilots were installed in the model for the purpose of keeping the model flying straight and level in the tunnel.

In order to provide a stable test vehicle, the autopilot system had to perform adequately as a regulatory system which would keep the model flying within the confines of the tunnel, but still would allow the model to behave largely as a free body during flutter tests.

The model tested was a dynamically scaled fighter-type airplane with a wing of aspect ratio 3.45, 40° sweepback of the quarter-chord line, and a taper ratio of 0.578. In order to simplify the initial experimental tests, aeroelastic effects were avoided by using a set of rigid wing panels. An interchangeable set of flexible panels was provided for the wing flutter tests.

Flights were made in the 19-foot pressure tunnel at atmospheric pressure up to a maximum airstream velocity of 200 mph.

It is anticipated that the towed-model testing technique will be utilized to a greater extent than heretofore and that there will then be a need for information concerning the technique. This report is intended to demonstrate the feasibility of wind-tunnel testing by the towed-model technique at moderate subsonic speeds. Comparison of experimental lateral and longitudinal time histories of the model motion, for the model equipped with both the rigid wing panels and the flexible wing panels, is made with motions calculated on an analog computer. The lateral equations of motion for a towed airplane have been developed in reference 2, and the longitudinal equations of motion are developed in an appendix to the present paper. This comparison was made despite the knowledge that experimentally the model was excited by random disturbances of an unknown magnitude, so that the comparison was not orthodox. In addition, lateral periods and damping calculated for various autopilot conditions are included.

## SYMBOLS

All forces and moments are referred to the stability system of axes which is described in figure 1.

| | |
|---|---|
| $A,B,C,E,F,G$ | coefficients of the lateral-stability equation |
| $H,I,J,K$ | coefficients of the longitudinal-stability equation |
| $C_D$ | drag coefficient, $\frac{D}{q'S}$ |
| $C_L$ | lift coefficient, $\frac{L}{q'S}$ |

$C_m$ pitching-moment coefficient, $\frac{M}{q'S\bar{c}}$

$C_n$ yawing-moment coefficient, $\frac{N}{q'Sb}$

$C_l$ rolling-moment coefficient, $\frac{L'}{q'Sb}$

$C_W$ weight coefficient, $\frac{W}{q'S}$

$C_X$ towline longitudinal-force coefficient, $\frac{T_X}{q'S}$

$C_Y$ side-force coefficient, $\frac{Y}{q'S}$

$C_Z$ towline vertical-force coefficient, $\frac{T_Z}{q'S}$

$C_{l/2}$ cycles to damp to half amplitude, $\frac{T_{l/2}}{P}$

D drag force, lb

$D_b$ lateral differential operator, $\frac{d}{ds_b}$

$D_c$ longitudinal differential operator, $\frac{d}{ds_c}$

$I_{X_o}$ moment of inertia about principal X-axis, slug-ft$^2$

$I_{Y_o}$ moment of inertia about principal Y-axis, slug-ft$^2$

$I_{Z_o}$ moment of inertia about principal Z-axis, slug-ft$^2$

$I_X$ moment of inertia about X-axis, slug-ft$^2$

$I_Y$ moment of inertia about Y-axis, slug-ft$^2$

$I_Z$ moment of inertia about Z-axis, slug-ft$^2$

$I_{XZ}$ product of inertia, $-\left(I_{Z_O} - I_{X_O}\right) \cos \eta \sin \eta$

$K_X^2$ radius of gyration about X-axis, $\frac{I_X}{mb^2}$

$K_Y^2$ radius of gyration about Y-axis, $\frac{I_Y}{m\bar{c}^2}$

$K_Z^2$ radius of gyration about Z-axis, $\frac{I_Z}{mb^2}$

$K_{XZ}$ product-of-inertia factor, $\frac{I_{XZ}}{mb^2}$

$K_{\theta}'$ elevator-position-control gearing ratio, radians/radian

$K_{\dot{\theta}}$ pitch-damper gearing ratio, radians/radian/sec

$K_{\phi}$ roll-autopilot gearing ratio, radians/radian

$K_{\psi}'$ rudder-position-control gearing ratio, radians/radian

$K_{\dot{\psi}}$ yaw-damper gearing ratio, radians/radian/sec

L lift, lb

L' rolling moment, ft-lb

M pitching moment, ft-lb

N yawing moment, ft-lb

P period of oscillation, sec

S wing area, sq ft

T towline tension, lb

$T_{1/2}$ time required for oscillation to damp to one-half amplitude, sec

V tunnel airstream velocity, ft/sec

W model weight, lb

| | |
|---|---|
| $Y$ | side force, lb |
| $b$ | model wing span, ft |
| $c$ | model wing chord, ft |
| $\bar{c}$ | model wing mean aerodynamic chord, ft |
| $l$ | towline length, ft |
| $m$ | mass of model, slugs |
| $p$ | rolling velocity, $\frac{d\phi}{dt}$ |
| $q$ | pitching velocity, $\frac{d\theta}{dt}$ |
| $q'$ | tunnel dynamic pressure, $\frac{1}{2}\rho V^2$, lb/sq ft |
| $r$ | yawing velocity, $\frac{d\psi}{dt}$ |
| $s_b$ | nondimensional time parameter based on span, $\frac{Vt}{b}$ |
| $s_c$ | nondimensional time parameter based on mean aerodynamic chord, $\frac{Vt}{\bar{c}}$ |
| $t$ | time, sec |
| $u$ | nondimensional longitudinal perturbation velocity |
| $x'$ | distance along model center line from center of gravity to towline attachment point, positive forward of center of gravity, ft |
| $y$ | lateral displacement of model center of gravity, positive to the right, ft |
| $z$ | vertical displacement of model center of gravity from equilibrium, positive down, ft |
| $z'$ | vertical distance from X-axis to towline attachment point |

| | |
|---|---|
| $\alpha$ | perturbation angle of attack, radians |
| $\alpha'$ | angle of attack, radians |
| $\alpha_o$ | angle of attack in undisturbed condition, radians |
| $\dot{\alpha}$ | rate of change of angle of attack, $\frac{d\alpha}{dt}$ |
| $\beta$ | angle of sideslip, radians |
| $\gamma$ | flight-path angle, radians |
| $\delta_a$ | angle of aileron deflection perpendicular to aileron hinge line, positive to produce positive roll, radians |
| $\delta_e$ | angle of elevator deflection perpendicular to elevator hinge line, positive trailing edge down, radians |
| $\delta_r$ | angle of rudder deflection perpendicular to rudder hinge line, positive trailing edge left, radians |
| $\eta$ | inclination of principal longitudinal axis, radians |
| $\eta_o$ | inclination of principal longitudinal axis from fuselage center line, radians |
| $\theta$ | perturbation angle of pitch, radians |
| $\theta_o$ | angle of pitch in undisturbed condition, radians |
| $\theta'$ | angle between towline and model center line in xz-plane, radians |
| $\dot{\theta}$ | rate of change of angle of pitch, $\frac{d\theta}{dt}$ |
| $\lambda$ | angle between towline and horizontal, radians |
| $\mu_b$ | relative density factor based on span, $\frac{m}{\rho S b}$ |
| $\mu_c$ | relative density factor based on chord, $\frac{m}{\rho S \bar{c}}$ |
| $\xi$ | angle between towline and X-axis, radians |
| $\rho$ | tunnel airstream density, slugs/cu ft |

$\phi$ angle of roll, radians

$\psi$ angle of yaw, radians

$\dot{\psi}$ rate of change of angle of yaw, $\frac{d\psi}{dt}$

$\psi'$ angle between towline and model center line in xy-plane, radians

$\Omega$ total angle of pitch, $\theta_o + \theta$, radians

Aerodynamic coefficients and force coefficients with a subscript indicate the partial derivative of the quantity with respect to the indicated quantity nondimensionalized in the standard manner. For example,

$$C_{l_p} = \frac{\partial C_l}{\partial \frac{pb}{2V}} = \frac{\partial C_l}{\partial\left(\frac{b}{2V}\frac{d\phi}{dt}\right)}$$

## MODEL

The tests were made on a dynamically scaled model of a swept-wing fighter-type aircraft of current design. Pertinent model areas and dimensions are shown in figure 2 and are listed in table I. Table I also lists the scaled mass characteristics of the model. The fuselage and tail surfaces were constructed of a fiber glass and plastic laminate, wrapped around a shell of foam plastic for rigidity. The resultant structure was light, strong, and essentially rigid, and provided the housing for the autopilot system and the instrumentation.

Two interchangeable pairs of wing panels were provided for the model. One pair of panels was rigid and was constructed of aluminum sheets sandwiched between mahogany layers. The other pair of wing panels (described in detail in ref. 1) was constructed to have scaled stiffness, weight, and inertia characteristics and was, as a result, flexible. The bending and torsion strength of these flexible wing panels was concentrated in an aluminum spar. The airfoil contour was formed by independent balsa-wood pods which were attached to the spar. Full-chord wing fences were used on the model to improve the flow over the wing at low speeds. The fences were located at 68 percent of the wing span.

External stores were mounted below the wings as shown in figure 2. These stores provided a housing for gyroscopic flutter stoppers which provided mechanical damping to the wing at the operator's command. The

gyroscopes were air-driven and were mounted in gimbals normally free to move. A solenoid-operated air valve permitted the operator to restrain the gyroscope gimbals which provided a damping force which opposed the wing flutter motion.

## AUTOPILOT AND CONTROLS

Several mechanisms were incorporated in the model to keep it flying straight and level in the tunnel. Each of the mechanisms was independent of the other components, but all of the mechanisms as a group will be referred to as the autopilot in this paper. Each of the mechanisms individually will be discussed as a component of the autopilot.

Roll control.- To provide roll control, an electrically driven displacement gyroscope was mechanically linked to the ailerons. The linkage was such that any bank angle caused an aileron deflection which provided a restoring rolling moment. Mathematically, the roll component of the autopilot could be represented by the equation $\delta_a = -K_\phi \phi$, where $K_\phi$ is the gearing ratio ($\phi$ is the angle of roll about the model longitudinal axis). The value of the gearing ratio could be varied, but was fixed during any particular flight. A photograph of the gyroscope is shown in figure 3, and the gyroscope and linkage is shown schematically in figure 4. A description of the gyroscope can be found in reference 3 and the dynamic characteristics are presented in table II.

The gyroscope tended to drift away from the zero position owing to both friction in the bearings and aileron hinge moments. This gyroscopic drift produced an aileron deflection with a resultant model angle of bank. In order to compensate for the drift during flight, an electromagnetic precession coil was mounted so that a corrective torque could be applied to the inner gimbal of the gyroscope at the operator's command in such a manner as to cause the gyroscope to return to the zero position.

The ailerons were plain flaps with a chord of 25 percent of the wing chord perpendicular to the quarter chord. The aileron span extended from $0.155b/2$ to $0.517b/2$.

Automatic position control.- The towline was linked to the elevator and rudder in such a manner that a control-surface deflection was produced whenever the model center line was not alined with the towline. The linkage was such that the deflection produced a corrective moment to realine the model center line with the towline (see fig. 4). Mathematically, the deflection could be represented by the equations $\delta_e = K_{\theta'}\theta'$ and $\delta_r = K_{\psi'}\psi'$ where $K_{\theta'}$ and $K_{\psi'}$ are the gearing ratios and $\theta'$ and $\psi'$ are the angles between the towline and the model center line in

the yz- and xy-planes. The values of $K_\theta$, and $K_\psi$, could be varied, but were fixed during any flight.

The elevator segment connected to this linkage had a chord of 30 percent of the stabilizer chord and had a span extending from 7 to 50 percent of the stabilizer span. Similarly, the rudder segment connected to this linkage had a constant chord of 2.741 inches parallel to the fuselage center line and a span extending from 0.27 to 50 percent of the vertical tail span.

Pitch and yaw dampers.- The model aerodynamic damping in pitch and damping in yaw were augmented by rate-gyro—servo units. These units provided elevator or rudder deflections proportional to the pitching and yawing velocities, respectively, which caused moments which opposed the motion, thus providing artificial damping. The dampers can be represented mathematically by the equations $\delta_e = K_{\dot\theta}\dot\theta$ and $\delta_r = K_{\dot\psi}\dot\psi$ where $K_{\dot\theta}$ and $K_{\dot\psi}$ are the gain constants, and $\dot\theta$ and $\dot\psi$ are the pitching and yawing velocities. The values of $K_{\dot\theta}$ and $K_{\dot\psi}$ could be varied during flight. Schematic representation of the rate-gyro—servo units and the linkages are shown in figure 4 and a description can be found in reference 4. The dynamic characteristics of these units are listed in table II.

The pitch damper was linked to the outboard segment of the elevator (span extending from 50 percent to 100 percent of the horizontal stabilizer span) and had a chord of 30 percent of the stabilizer chord.

The yaw damper was linked to the upper segment of the rudder (span extending from 50 percent to 88 percent of the vertical stabilizer span) and had a chord of 2.741 inches, parallel to the fuselage center line.

Manual vertical position control.- During airspeed changes, the model was kept at or near the tunnel center line (vertically) by varying the deflection of the inner segment of the elevator (the segment linked to the automatic position control). A small electric motor was incorporated in the automatic position control linkage in such a manner as to vary the length of a push rod, at the operator's command, thereby changing the elevator deflection. This manual control was also used to take off and land the model.

## TESTING EQUIPMENT

The towline was 38 feet long (6.8b) from the point of attachment at the nose to the restraining yoke. The yoke was in the entrance cone of

the tunnel and was restrained longitudinally by a drag cable attached to the tunnel turning vanes. (See fig. 5.) Vertical and lateral motions of the yoke were restrained by three cables which fixed the yoke on the tunnel center line.

The towline consisted of 35 feet of 1/16-inch flexible aircraft cable plus a 3-foot aluminum rod attached to a universal joint at the nose of the model. The aluminum rod was required to provide a moment at the universal joint to oppose the control-surface hinge moment. A bundle of electrical leads and a flexible plastic air supply tube was attached to the aircraft cable from the yoke to the model. The leads provided electrical power to the model and transmitted data from the instruments. The air supply tube provided air which was required for the flutter-stopper gyroscopes and for the rate-gyro—servo units. The total weight of the towline, leads, and air tube was about 3.5 pounds.

A flat rubber padded platform provided a landing mat. (See fig. 5.) A bubble canopy was installed in the tunnel floor to the rear of the test section to provide an observation point for the aileron trim operator. As a safety feature, a model hold-down wire was provided to keep the model on the landing mat before and after the flights. This wire consisted of 1/16-inch aircraft cable attached at the bottom of the fuselage just below the center of gravity. The cable was conducted out of the tunnel to an operator who provided the pull required to keep the model on the floor. During flight, the wire was kept slack.

The model motions were recorded by three motion-picture cameras placed at the top, side, and rear of the tunnel test section. Instrumentation in the model provided information as to the model accelerations and the flexible wing panel motions (see ref. 1) and the control-surface deflections. These data were recorded on an oscillograph but are not presented.

A timing device (which indicated on the camera film and on the oscillograph records) enabled the two sets of data to be correlated with respect to time.

Data were recorded at 100 mph and at the maximum speed of each flight.

## TESTING PROCEDURE

The model was placed on the landing mat in a position which put tension into the tow cable approximately equal to the model drag at take-off. All controls and instruments were started before the tunnel drive motor was started. The elevator was positioned so as to hold the

model on the mat, and tension was applied to the hold-down wire. When the tunnel airspeed reached approximately 100 mph, up elevator was applied until the model rose from the mat to approximately the center of the tunnel. The tunnel airspeed was then slowly increased and the elevator trim angle was varied manually to keep the model close to the tunnel center horizontally. If the model deviated too far from the tunnel center laterally owing to drift in the roll-control gyroscope, the precession device was energized to return the model to the center. (The model rarely remained stationary in the tunnel so that trim control was applied only when it was evident that the model was oscillating about some location to the side of the tunnel center.)

In general, the flights with the rigid wing model were terminated at the speeds at which the model motions were considered to be of such large amplitudes that the model was in danger of being destroyed. At such a time the model was landed after the tunnel airspeed was reduced to 100 mph. The gearing ratio of one of the autopilot components was then changed, and the model flight test repeated. This process continued on a trial basis until a set of autopilot gearing ratios was found which gave satisfactory flights at speeds up to 200 mph, the maximum speed of the tests. Some difficulty was encountered during this process in that the gearing ratios found to give good flights at low speeds were found to give unsatisfactory flights at high speeds. The converse trend was observed as well. However, compromise gearing ratios were found which permitted the model to be flown at both low and high speeds.

For the model equipped with the flexible wings, the process was the same except that the maximum speed was the wing flutter speed. (The wing flutter speed (ref. 1) was varied by moving weights in the external stores.) It should be mentioned that the flying characteristics of the rigid and flexible wing models were not identical (because of aeroelasticity) so that the gearing ratios used for the rigid wing model had to be readjusted for the flights with the flexible wing panels.

## CALCULATIONS

The equations of motion for the towed model, including the autopilot components, are presented in the appendix. As mentioned, the lateral equations of motion were obtained from reference 2. The aerodynamic coefficients used in the investigation are listed in table III. The static derivatives were obtained using the experimental data of reference 5 and unpublished data, and the rotary derivatives were obtained using the procedures of references 6 to 8. Model mass parameters (mass, moments of inertia, center-of-gravity location, and inclination of the principal axis) were determined experimentally by swinging and weighing the model.

Lateral and longitudinal dynamic stability studies were made on an analog computer to obtain time histories of the model motions. An initial condition was used to start the motions. For the lateral motions, a sidewise displacement in $y$ was used as an initial condition, whereas for the longitudinal motions, a vertical displacement $z$ was used. All initial velocities, accelerations, and other displacements were assumed to be zero.

The roots of the lateral equations of motion were also obtained on an electronic calculator to define the periods and damping of the model-autopilot combination better.

## RESULTS AND DISCUSSION

Systematic calculations of the period and cycles to damp to half amplitude have been made to show the effects of the autopilot gearing ratios. The results of the analytic study, for the lateral modes with three degrees of freedom of the rigid wing model at 145 ft/sec, are shown in figure 6. Three modes of motion are evident, and they are designated, for convenience, as the long-, middle-, and short-period motions. The effects of changes in $K_{\psi'}$, $K_{\phi}$, and $K_{\dot{\psi}}$ on the calculated periods and cycles to damp to half amplitude are shown. Some experimental periods are shown for comparison. For the case of $K_{\phi}$, the curves are shown dotted in the range $1/4 < K_{\phi} < 3/4$ since no points were calculated between those values and the dotted line represents the probable curve.

In an attempt to approximate some of the model characteristics, a one-degree-of-freedom (in roll) analysis was made; the results of which are shown in figure 6. It can be seen that the middle period is fairly well predicted (for $K_{\phi}$ between about 1/2 to 2), but the damping information shows a total lack of agreement with the three-degree-of-freedom analysis.

Typical time histories of the rigid wing model motion are shown in figure 7. A power spectrum density analysis of the angle of roll $\phi$ was conducted in an attempt to find the natural frequencies. Since the motions were influenced by the tunnel excitations, the natural frequencies were difficult to isolate from the forced frequencies. Figure 8 shows a typical power-spectrum-density analysis to illustrate the difficulties involved. However, the frequencies which were selected as being the natural frequencies are presented in table IV. The frequencies were chosen on the basis of this analysis and a judicious examination of the time histories to select any relatively undisturbed portion of the data. The periods of the natural frequencies of both the lateral and longitudinal degrees of freedom are shown (periods for the longitudinal modes

were obtained from the time histories exclusively). It can be seen that no general statement as to the reliability of the calculations can be formulated since the agreement varies from good to bad, and it is not clear whether the lack of correlation stems from inadequacies of the theoretical approach, inaccuracies in determining the stability derivatives, or from the inability to isolate the natural from the forced modes of motion.

Figure 9 shows the motions of the flexible wing model under the influence of the tunnel disturbances. It can be seen that, in general, the amplitudes of the motions are somewhat greater than when the model is equipped with the rigid wing panels.

As previously mentioned, the model apparently was continuously excited by unknown tunnel airstream disturbances during the flights, so that quantitative determination of the model damping characteristics was precluded. However, on the basis of visual observation, the operators evaluated the effects of autopilot gearing ratio changes on the model damping. In general, these deductions confirmed the calculated effects of $K_{\psi}$, and $K_{\dot{\psi}}$ on the damping shown in figure 6. However, the calculated indications that changes in $K_{\phi}$ (above $K_{\phi} \approx 1$) did not materially affect the cycles to damp were not observed. The operators felt that increases in $K_{\phi}$ improved the long-period damping.

To illustrate the records obtained by an analog computer using the stability equations in the appendix, figure 10 shows the calculated time histories of the rigid wing model following an initial disturbance in y and z. The use of this initial condition was necessitated by the lack of knowledge of the actual forcing function, as previously discussed. However, the studies were of use for rapid determination of the trends of gearing ratios for stable flights.

## CONCLUDING REMARKS

Exploratory wind-tunnel tests of a towed airplane model equipped with an autopilot demonstrated the ability of the autopilot system to control the model at speeds up to 200 mph.

In seeking to make a comparison between the results of the theoretical and experimental investigations, it must be recognized that the natural frequencies may be obscured by the forcing frequencies of the tunnel airstream disturbances, so that any differences in the results may be a result of the experimental data, as well as inaccuracies in the theory or the derivatives. Visual observation of the experimental trends qualitatively confirmed the calculated variation of damping as the

autopilot gains $K_{\psi}$, and $K_{\dot{\psi}}$ were changed. However, the calculated effects of changes in $K_{\phi}$ were not visually confirmed.

The calculations predicted three oscillations in the lateral degrees of freedom and two oscillations in the longitudinal degrees of freedom. These results were confirmed experimentally.

Langley Aeronautical Laboratory,
National Advisory Committee for Aeronautics,
Langley Field, Va., December 14, 1954.

# APPENDIX

## EQUATIONS OF MOTION OF A TOWED AIRPLANE

The equations of motion of the towed airplane have been determined with respect to the stability axes (fig. 1). In order to simplify the equations and to facilitate the mathematical solutions, the following assumptions are made:

(1) All motions are perturbations from the equilibrium condition; thus, squares, higher-order terms, and products of the perturbations may be neglected. All angles are assumed small.

(2) The airplane is initially flying with no roll or yaw and is in unaccelerated flight.

(3) The basic aerodynamic parameters are constant during any motion.

(4) The flow is quasi-steady; that is, any change in attitude produces an instantaneous change in forces.

(5) The towline is always straight.

(6) The towline is weightless and infinitely flexible and has no effect on the airplane other than that caused by direct forces and moments resulting from the towline tension.

(7) The lateral and longitudinal motions for the towed airplane are independent and may be considered separately, as for the free airplane.

### Lateral Equations of Motion

The lateral equations of motion for a towed airplane were derived in reference 2 and they are repeated here, in slightly different form, for completeness.

$$\left.\begin{aligned}
&\left(2\mu_b D_b - C_{Y_\beta} + \frac{C_D b}{2D_b}\right)\beta + \left[\left(2\mu_b - \frac{C_{Y_r}}{2}\right)D_b + C_D\left(1 + \frac{x'}{l}\right) + \frac{C_D b}{2D_b}\right]\psi + \\
&\left(-\frac{C_{Y_p}}{2} D_b - C_W + C_D\frac{z'}{l}\right)\phi = C_{Y_{\delta_r}}\delta_r \\
&\left(-C_{n_\beta} + \frac{C_D x'}{2D_b}\right)\beta + \left[2\mu_b K_Z{}^2 D_b{}^2 - \frac{C_{n_r}}{2} D_b + C_D\frac{x'}{b}\left(1 + \frac{x'}{l}\right) + \frac{C_D x'}{2D_b}\right]\psi + \\
&\left(-2\mu_b K_{XZ} D_b{}^2 - \frac{C_{n_p}}{2} D_b + C_D\frac{x'z'}{bl}\right)\phi = C_{n_{\delta_r}}\delta_r + C_{n_{\delta_a}}\delta_a \\
&\left(-C_{l_\beta} + \frac{C_D z'}{2D_b}\right)\beta + \left[-2\mu_b K_{XZ} D_b{}^2 - \frac{C_{l_r}}{2} D_b + C_D\frac{z'}{b}\left(1 + \frac{x'}{l}\right) + C_D\frac{z'}{2D_b}\right]\psi + \\
&\left(2\mu_b K_X{}^2 D_b{}^2 - \frac{C_{l_p}}{2} D_b + C_D\frac{z'^2}{2b}\right)\phi = C_{l_{\delta_r}}\delta_r + C_{l_{\delta_a}}\delta_a
\end{aligned}\right\} \quad (A1)$$

The determinant of the characteristic lateral-stability equations yields a ninth-order equation, with three zero roots. After the zero roots are dropped, the equation is of the form

$$D_b{}^6 + AD_b{}^5 + BD_b{}^4 + CD_b{}^3 + ED_b{}^2 + FD_b + G = 0 \quad (A2)$$

For a detailed derivation of the equations, see reference 2.

In addition to the airplane-stability equations, the following equations were used to represent the various autopilot components:

Roll control.-

$$\delta_a = -K_\phi\phi \quad (A3)$$

Lateral automatic position control plus yaw damper.-

$$\delta_r = K_{\psi'}\psi' + K_{\dot{\psi}}\dot{\psi}$$

or, in operator form,

$$\delta_r = K_{\psi'}\left[\left(1 + \frac{x'}{l}\right)\psi + \frac{(\beta + \psi)}{D_b}\frac{b}{l}\right] + K_{\dot{\psi}}\frac{V}{b}D_b\psi \qquad (A4)$$

where the towline angle $\psi'$ is approximated by

$$\psi' = \left(1 + \frac{x'}{l}\right)\psi + \frac{y}{l} = \left(1 + \frac{x'}{l}\right)\psi + \frac{\beta + \psi}{D_b}\frac{b}{l}$$

For the frequency range of interest for these computations, the representation of the roll control and yaw damper by ideal first-order equations is permissible since the response characteristics are linear in the low-frequency range.

The roll-control gyro and the yaw-damper rate-gyro were, of course, fixed to the model. The quantities to which they responded were actually the roll about the body axis and the yawing velocity about the body axis, rather than roll and yaw about the corresponding stability axis. However, since the angle of attack was small, it was felt that it would complicate the equations unnecessarily to transfer these quantities to the stability axis system for this investigation. It was assumed then that the two autopilot components responded to the quantities about the stability axes.

## Longitudinal Equations of Motion

The basic longitudinal equations of motion for a free airplane with three degrees of freedom were modified to include the effect of the towline forces and moments. No attempt has been made to analyze the dynamics of the towline other than to include the effect of the forces on the airplane.

Figure 11 shows a schematic representation of the towed airplane in a disturbed condition and will be used as an aid in developing the equations of motion. It should be noted that the total instantaneous angle of attack

$$\alpha' = \alpha_o + \alpha$$

and that the total instantaneous angle of pitch

$$\Omega = \theta_o + \theta$$

and finally that

$$\alpha_o = \theta_o$$

since the airplane is assumed to be in level flight in the undisturbed conditions. It should be noted that with the axes system being used (stability axes), the X-axis is fixed to one given position (the direction of the undisturbed airstream) to the body during any disturbed motion.

The longitudinal equations of motion for a towed airplane may be written as follows:

$$\left.\begin{aligned}
&\frac{2I_Y}{\rho S\bar{c}^3} D_c{}^2\theta = C_{m_{D_c\theta}} D_c\theta + \left(C_{m_{D_c\alpha}} D_c + C_{m_\alpha}\right)\alpha + C_{m_u} u + \\
&\qquad C_{m_{\delta_e}}\delta_e + \left(C_{m_\theta}\right)_T\theta + \left(C_{m_\alpha}\right)_T\alpha + \left(C_{m_u}\right)_T u + \left(C_{m_z}\right)_T z \\
&\frac{2m}{\rho S\bar{c}} D_c\alpha = \left(\frac{2m}{\rho S\bar{c}} - C_{L_{D_c\theta}}\right) D_c\theta - C_{L_\alpha}\alpha - 2C_L u - C_{L_{\delta_e}}\delta_e + \\
&\qquad \left(C_{Z_\theta}\right)_T\theta + \left(C_{Z_u}\right)_T u + \left(C_{Z_\alpha}\right)_T\alpha + \left(C_{Z_z}\right)_T z \\
&\frac{2m}{\rho S\bar{c}} D_c u = -C_L\theta - \left(C_{D_\alpha} - C_L\right)\alpha + 2C_D u + \left(C_{X_\theta}\right)_T\theta + \\
&\qquad \left(C_{X_\alpha}\right)_T\alpha + \left(C_{X_u}\right)_T u + \left(C_{X_z}\right)_T z
\end{aligned}\right\} \quad (A5)$$

where the coefficients with the subscript T represent the forces and moments due to the towline tension. It is these quantities which must be determined.

To simplify the writing of the equations and to transform them into familiar notation, let

$$\mu_c = \frac{m}{\rho S \bar{c}}$$

$$K_Y{}^2 = \frac{I_Y}{m\bar{c}^2}$$

$$C_{m_{D_c\theta}} = \frac{C_{m_q}}{2}$$

$$C_{m_{D_c\alpha}} = \frac{C_{m_{\dot{\alpha}}}}{2}$$

$$C_{L_{D_c\theta}} = \frac{C_{L_q}}{2}$$

Substituting these values into equations (A5) leads to:

$$\left.\begin{aligned}
2\mu_c K_Y{}^2 D_c{}^2\theta &= \frac{C_{m_q}}{2} D_c\theta + \left(\frac{C_{m_{\dot{\alpha}}}}{2} D_c + C_{m_\alpha}\right)\alpha + C_{m_u} u + \\
&\quad C_{m_{\delta_e}}\delta_e + \left(C_{m_\theta}\right)_T\theta + \left(C_{m_\alpha}\right)_T\alpha + \left(C_{m_u}\right)_T u + \left(C_{m_z}\right)_T z \\
2\mu_c D_c\alpha &= \left(2\mu_c - \frac{C_{L_q}}{2}\right)D_c\theta - C_{L_\alpha}\alpha - 2C_L u - C_{L_{\delta_e}}\delta_e + \\
&\quad \left(C_{Z_\theta}\right)_T\theta + \left(C_{Z_\alpha}\right)_T\alpha + \left(C_{Z_u}\right)_T u + \left(C_{Z_z}\right)_T z \\
2\mu_c D_c u &= -C_L\theta - \left(C_{D_\alpha} - C_L\right)\alpha - 2C_D u + \left(C_{X_\theta}\right)_T\theta + \\
&\quad \left(C_{X_\alpha}\right)_T\alpha + \left(C_{X_u}\right)_T u + \left(C_{X_z}\right)_T z
\end{aligned}\right\}$$

The towline terms $C_X$, $C_Z$, and $C_m$ must be determined to substitute in equations (A6). Referring to figure 11, it can be seen that

$$\lambda = \sin^{-1}\frac{z'}{l}$$

$$= \sin^{-1}\left(\frac{z}{l} - \frac{x' \sin \Omega}{l}\right)$$

or, with the sines replaced by the angles,

$$\lambda \approx \frac{z}{l} - \frac{x'\Omega}{l} = \frac{z}{l} - \frac{x'}{l}\left(\theta_o + \theta\right) \tag{A7}$$

Now the airplane was assumed to have initially been in level flight so that

$$\xi = \lambda - \theta$$

$$\xi = \frac{z}{l} - \frac{x'}{l}\theta_o - \left(1 + \frac{x'}{l}\right)\theta \tag{A8}$$

which is the angle between the towline and the X-axis.

Consider the towline force along the X-axis:

$$T_X = T \cos \xi$$

Within the approximation of small angles, this can be replaced by

$$T_X \approx T \tag{A9}$$

Along the Z-axis, the towline forces are

$$T_Z = -T \sin \xi$$

or again the approximation

$$T_Z \approx -T\xi \tag{A10}$$

In normal level flight with the assumption of small disturbances, it can be assumed that

$$T \approx D = C_D S q' \equiv C_{D_\alpha} \alpha' S q'$$

Equations (A9) and (A10) now become

$$T_X = C_{D_\alpha} \alpha' S q' \tag{A11}$$

$$T_Z = -C_{D_\alpha} \alpha' S q' \xi = -C_{D_\alpha} \alpha' S q' \left[ \frac{z}{l} - \frac{x'}{l} \theta_o - \left( 1 + \frac{x'}{l} \right) \theta \right] \tag{A12}$$

Since the towline is attached to the nose of the airplane, at x', away from the center of gravity, the towline forces produce a moment about the Y-axis. This moment can be expressed as

$$M_T = -T_X x' \sin \theta_o - T_Z x' \cos \theta_o$$

$$M_T \approx -T_X x' \theta_o - T_Z x' \tag{A13}$$

Substituting equations (A11) and (A12) into (A13)

$$M_T = -x' \left( C_{D_\alpha} \alpha' \frac{\rho}{2} S V^2 \theta_o \right) + x' \left( C_{D_\alpha} \alpha' \frac{\rho}{2} S V^2 \right) \left[ \frac{z}{l} - \frac{x'}{l} \theta_o - \left( 1 + \frac{x'}{l} \right) \theta \right]$$

$$M_T = -x' \frac{\rho}{2} S C_{D_\alpha} \alpha' V^2 \left[ \theta_o \left( 1 + \frac{x'}{l} \right) - \frac{z}{l} + \theta \left( 1 + \frac{x'}{l} \right) \right] \tag{A14}$$

The towline longitudinal force and moment derivatives can be found by differentiating equations (A11), (A12), and (A14) with respect to the desired variable.

Consider the X-forces:

$$T_{X_\alpha} = \frac{\partial T_X}{\partial \alpha} = \frac{\partial}{\partial \alpha}\left(C_{D_\alpha}\alpha' \frac{\rho}{2} V^2 S\right) = C_{D_\alpha} \frac{\rho}{2} V^2 S \tag{A15}$$

In coefficient form

$$\left(C_{X_\alpha}\right)_T = \frac{T_{X_\alpha}}{q'S} = C_{D_\alpha} \tag{A16}$$

Similarly,

$$T_{X_\theta} = \frac{\partial T_X}{\partial \theta} = \frac{\partial}{\partial \theta}\left(C_{D_\alpha}\alpha' \frac{\rho}{2} V^2 S\right) = 0$$

then

$$\left(C_{X_\theta}\right)_T = 0 \tag{A17}$$

and the force due to velocity is

$$T_{X_V} = \frac{\partial T_X}{\partial V} = \frac{\partial}{\partial V}\left(C_{D_\alpha}\alpha' \frac{\rho}{2} V^2 S\right) = C_{D_\alpha}\alpha'\rho VS = C_D \rho VS$$

which in coefficient form is

$$\left(C_{X_V}\right)_T = \frac{2C_D}{V}$$

or

$$\left(C_{X_u}\right)_T = V\left(C_{X_V}\right)_T = 2C_D \tag{A18}$$

Also

$$T_{X_z} = \frac{\partial T_X}{\partial z} = \frac{\partial}{\partial z}\left(C_{D_\alpha}\alpha' \frac{\rho}{2} V^2 S\right) = 0$$

then

$$\left(C_{X_Z}\right)_T = 0 \tag{A19}$$

It is recognized that for towed-model testing in a wind tunnel, V could be neglected as a variable. For possible application to towed-gliders problems, V is retained as a variable at this time.

Similarly, for the Z-forces:

$$T_{Z_\alpha} = \frac{\partial T_Z}{\partial \alpha}$$

$$= \frac{\partial}{\partial \alpha}\left\{-C_{D_\alpha}\alpha' \frac{\rho}{2} V^2 S\left[\frac{z}{l} - \frac{x'}{l}\theta_o - \left(1 + \frac{x'}{l}\right)\theta\right]\right\}$$

$$= -C_{D_\alpha} \frac{\rho}{2} V^2 S\left[\frac{z}{l} - \frac{x'}{l}\theta_o - \left(1 + \frac{x'}{l}\right)\theta\right]$$

or, in coefficient form,

$$\left(C_{Z_\alpha}\right)_T = -C_{D_\alpha}\left[\frac{z}{l} - \frac{x'}{l}\theta_o - \left(1 + \frac{x'}{l}\right)\theta\right] \tag{A20}$$

The use of this coefficient $\left(C_{Z_\alpha}\right)_T$ would, of course, result in nonlinear equations since the coefficient is dependent upon both $z$ and $\theta$. Thus, to maintain the assumption of linear equations, let

$$\left(C_{Z_\alpha}\right)_T \approx C_{D_\alpha} \frac{x'}{l}\theta_o \tag{A21}$$

It should be noted that the $z$ and $\theta$ terms can be larger than the $\theta_o$ term.

Similarly,

$$T_{Z_\theta} = \frac{\partial T_Z}{\partial \theta} = \frac{\partial}{\partial \theta}\left\{-C_{D_\alpha}\alpha' \frac{\rho}{2} SV^2\left[\frac{z}{l} - \frac{x'}{l}\theta_o - \left(1 + \frac{x'}{l}\right)\right]\theta\right\} = C_{D_\alpha}\alpha' \frac{\rho}{2} SV^2\left(1 + \frac{x'}{l}\right)$$

then

$$\left(C_{Z_\theta}\right)_T = C_{D_\alpha}\alpha'\left(1 + \frac{x'}{l}\right) = C_D\left(1 + \frac{x'}{l}\right) \tag{A22}$$

also,

$$T_{Z_V} = \frac{\partial T_Z}{\partial V} = \frac{\partial}{\partial V}\left\{-C_{D_\alpha}\alpha' \frac{\rho}{2} V^2 S\left[\frac{z}{l} - \frac{x'}{l}\theta_o - \left(1 + \frac{x'}{l}\right)\theta\right]\right\} = -C_{D_\alpha}\alpha'\rho VS\left[\frac{z}{l} - \frac{x'}{l}\theta_o - \left(1 + \frac{x'}{l}\right)\theta\right]$$

then,

$$\left(C_{Z_V}\right)_T = -\frac{2C_{D_\alpha}\alpha'}{V}\left[\frac{z}{l} - \frac{x'}{l}\theta_o - \left(1 + \frac{x'}{l}\right)\theta\right] = -\frac{2C_D}{V}\left[\frac{z}{l} - \frac{x'}{l}\theta_o - \left(1 + \frac{x'}{l}\right)\theta\right]$$

or

$$\left(C_{Z_u}\right)_T = V\left(C_{Z_V}\right)_T = -2C_D\left[\frac{z}{l} - \frac{x'}{l}\theta_o - \left(1 + \frac{x'}{l}\right)\theta\right]$$

As before, this must be simplified to

$$\left(C_{Z_u}\right)_T = 2C_D \frac{x'}{l}\theta_o \tag{A23}$$

The force

$$T_{Z_z} = \frac{\partial T_Z}{\partial z} = \frac{\partial}{\partial z}\left\{-C_{D_\alpha}\alpha' \frac{\rho}{2} V^2 S \left[\frac{z}{l} - \frac{x'}{l}\theta_o - \left(1 + \frac{x'}{l}\right)\theta\right]\right\} = -C_{D_\alpha}\alpha' \frac{\rho}{2} V^2 S \frac{1}{l} = -C_D \frac{\rho}{2} V^2 S \frac{1}{l}$$

reduces to coefficient form as

$$\left(C_{Z_z}\right)_T = \frac{-C_D}{l} \tag{A24}$$

The pitching-moment derivatives due to the towline can be found from equation (A14):

$$M_{T_\alpha} = \frac{\partial M_T}{\partial \alpha} = \frac{\partial}{\partial \alpha}\left\{-\frac{\rho}{2} V^2 S C_{D_\alpha}\alpha' x' \left[\left(\theta_o + \theta\right)\left(1 + \frac{x'}{l}\right) - \frac{z}{l}\right]\right\}$$

$$= -\frac{\rho}{2} V^2 S C_{D_\alpha} x' \left[\left(\theta_o + \theta\right)\left(1 + \frac{x'}{l}\right) - \frac{z}{l}\right]$$

or

$$\left(C_{m_\alpha}\right)_T = \frac{M_{T_\alpha}}{\frac{\rho}{2} V^2 S \bar{c}} = -C_{D_\alpha} \frac{x'}{\bar{c}} \left[\left(\theta_o + \theta\right)\left(1 + \frac{x'}{l}\right) - \frac{z}{l}\right]$$

As before, neglecting the terms which will be products of small disturbances, so that linearity will be preserved,

$$\left(C_{m_\alpha}\right)_T \approx -C_{D_\alpha} \frac{x'}{\bar{c}} \theta_o \left(1 + \frac{x'}{l}\right) \tag{A25}$$

Similarly

$$M_{T_\theta} = \frac{\partial M_T}{\partial \theta} = \frac{\partial}{\partial \theta}\left\{-\frac{\rho}{2} V^2 S C_{D_\alpha} \alpha' x' \left[\left(\theta_o + \theta\right)\left(1 + \frac{x'}{l}\right) - \frac{z}{l}\right]\right\}$$

$$= -\frac{\rho}{2} V^2 S C_{D_\alpha} \alpha' x' \left(1 + \frac{x'}{l}\right) = -\frac{\rho}{2} V^2 S C_D x' \left(1 + \frac{x'}{l}\right)$$

then

$$\left(C_{m_\theta}\right)_T = -C_D \frac{x'}{\bar{c}}\left(1 + \frac{x'}{l}\right) \tag{A26}$$

also,

$$M_{T_V} = \frac{\partial M_T}{\partial V} = \frac{\partial}{\partial V}\left\{-\frac{\rho}{2} V^2 S C_{D_\alpha} \alpha' x' \left[\left(\theta_o + \theta\right)\left(1 + \frac{x'}{l}\right) - \frac{z}{l}\right]\right\}$$

$$= -\rho V S C_{D_\alpha} \alpha' x' \left[\left(\theta_o + \theta\right)\left(1 + \frac{x'}{l}\right) - \frac{z}{l}\right]$$

$$= -\rho V S C_D x' \left[\left(\theta_o + \theta\right)\left(1 + \frac{x'}{l}\right) - \frac{z}{l}\right]$$

then,

$$\left(C_{m_V}\right)_T = -\frac{2C_D}{V} \frac{x'}{\bar{c}} \left[\left(\theta_o + \theta\right)\left(1 + \frac{x'}{l}\right) - \frac{z}{l}\right]$$

or

$$\left(C_{m_u}\right)_T = -2C_D \frac{x'}{\bar{c}} \left[\left(\theta_o + \theta\right)\left(1 + \frac{x'}{l}\right) - \frac{z}{l}\right]$$

Again neglecting potential products of small disturbances,

$$\left(C_{m_u}\right)_T = -2C_D \frac{x'}{\bar{c}}\left(1 + \frac{x'}{l}\right)\theta_o \tag{A27}$$

when

$$M_{T_z} = \frac{\partial M_T}{\partial z} = \frac{\partial}{\partial z}\left\{-\frac{\rho}{2} V^2 S C_{D_\alpha} \alpha' x' \left[\left(\theta_o + \theta\right)\left(1 + \frac{x'}{l}\right) - \frac{z}{l}\right]\right\} = \frac{\rho}{2} V^2 S x' C_{D_\alpha} \alpha' \frac{1}{l}$$

the coefficient form is

$$\left(C_{m_z}\right)_T = C_{D_\alpha} \alpha' \frac{x'}{\bar{c}} \frac{1}{l} = C_D \frac{x'}{\bar{c}} \frac{1}{l} \tag{A28}$$

Now inserting equations (A16) to (A19) and (A21) to (A28) into equations (A6), the following expressions are obtained:

$$\left.\begin{aligned}
2\mu_c K_Y{}^2 D_c{}^2\theta &= \left[\frac{C_{m_q}}{2} D_c - \frac{x'}{\bar{c}} C_D\left(1 + \frac{x'}{l}\right)\right]\theta + \left[\frac{C_{m_{\dot{\alpha}}}}{2} D_c + C_{m_\alpha} - \right. \\
&\left. \frac{x'}{\bar{c}} C_{D_\alpha}\theta_o\left(1 + \frac{x'}{l}\right)\right]\alpha + \left[C_{m_u} - 2\frac{x'}{\bar{c}} C_D\theta_o\left(1 + \frac{x'}{l}\right)\right] u + \\
&\frac{x'}{\bar{c}} \frac{C_D}{l} z + C_{m_{\delta_e}}\delta_e \\
2\mu_c D_c\alpha &= \left[\left(2\mu_c - \frac{C_{L_q}}{2}\right) D_c + C_D\left(1 + \frac{x'}{l}\right)\right]\theta + \left(-C_{L_\alpha} + C_{D_\alpha}\frac{x'}{l}\theta_o\right)\alpha + \\
&\left(-2C_L + \frac{2x'}{l}\theta_o C_D\right) u - \frac{C_D}{l} z - C_{L_{\delta_e}}\delta_e \\
2\mu_c D_c u &= -C_L\theta + \left(C_L - C_{D_\alpha} + C_{D_\alpha}\right)\alpha + \left(2C_D - 2C_D\right) u
\end{aligned}\right\} \tag{A29}$$

The last equation in equations (A29) can obviously be reduced so equations (A29) become

$$\left.\begin{aligned}
2\mu_c K_Y^2 D_c^2\theta &= \left[\frac{C_{m_q}}{2} D_c - \frac{x'}{\bar{c}} C_D\left(1 + \frac{x'}{l}\right)\right]\theta + \left[\frac{C_{m_{\dot{\alpha}}}}{2} D_c + C_{m_\alpha} - \right. \\
&\left. \frac{x'}{\bar{c}} C_{D_\alpha}\theta_o\left(1 + \frac{x'}{l}\right)\right]\alpha + \left[C_{m_u} - 2\frac{x'}{\bar{c}} C_D\theta_o\left(1 + \frac{x'}{l}\right)\right]u + \\
&\frac{x'}{\bar{c}} \frac{C_D}{l} z + C_{m_{\delta_e}}\delta_e \\
2\mu_c D_c\alpha &= \left[\left(2\mu_c - \frac{C_{L_q}}{2}\right)D_c + C_D\left(1 + \frac{x'}{l}\right)\right]\theta + \left(-C_{L_\alpha} + C_{D_\alpha}\frac{x'}{l}\theta_o\right)\alpha + \\
&\left(-2C_L + \frac{2x'}{l}\theta_o C_D\right)u - \frac{C_D}{l} z - C_{L_{\delta_e}}\delta_e \\
2\mu_c D_c u &= -C_L\left(\theta - \alpha\right)
\end{aligned}\right\} \quad \text{(A30)}$$

Letting

$$z = -V\int(\Omega - \alpha')dt$$

$$= -V\int\left(\theta_o - \alpha_o\right)dt - V\int(\theta - \alpha)dt$$

and remembering that the airplane was assumed to be in level flight, so that $\alpha_o = \theta_o$, leads to

$$-V \int \left(\theta_o - \alpha_o\right) dt = 0$$

Then

$$z = -V \int (\theta - \alpha) dt$$

or in operator form

$$z = - \frac{\bar{c}(\theta - \alpha)}{D_c}$$

Inserting this into equations (A30) gives

$$\left.\begin{aligned}
2\mu_c K_Y{}^2 D_c{}^2 \theta = {} & \left[\frac{C_{m_q}}{2} D_c - \frac{x'}{\bar{c}} C_D \left(1 + \frac{x'}{l}\right) - \frac{x'}{l} \frac{C_D}{D_c}\right]\theta + \left[\frac{C_{m_{\dot{\alpha}}}}{2} D_c + C_{m_\alpha} - \right. \\
& \left. \frac{x'}{\bar{c}} C_{D_\alpha} \theta_o \left(1 + \frac{x'}{l}\right) + \frac{x'}{l} \frac{C_D}{D_c}\right]\alpha + \left[C_{m_u} - \right. \\
& \left. 2 \frac{x'}{\bar{c}} C_D \theta_o \left(1 + \frac{x'}{l}\right)\right] u + C_{m_{\delta_e}} \delta_e \\
2\mu_c D_c \alpha = {} & \left[\left(2\mu_c - \frac{C_{L_q}}{2}\right) D_c + C_D \left(1 + \frac{x'}{l}\right) + \frac{C_D \bar{c}}{l} \frac{1}{D_c}\right]\theta + \\
& \left(-C_{L_\alpha} + C_D \frac{x'}{l} \theta_o - \frac{\bar{c}}{l} \frac{C_D}{D_c}\right)\alpha + \left(-2C_L + \frac{2x'}{l} \theta_o C_D\right) u - C_{L_{\delta_e}} \delta_e \\
2\mu_c D_c u = {} & -C_L \left(\theta - \alpha\right)
\end{aligned}\right\} \quad \text{(A31)}$$

The characteristic longitudinal-stability equation formed by the determinant of equations (A31) is a sixth-order equation, with two zero roots. The fourth-order equation which remains is of the form

$$D_c^4 + HD_c^3 + ID_c^2 + JD_c + K = 0$$

As mentioned previously, the equations of motion can be simplified by considering the forward velocity to be a constant. With this assumption, equations (A31) become

$$\left.\begin{aligned} 2\mu_c K_Y^2 D_c^2\theta = {} & \left[\frac{C_{m_q}}{2} D_c - \frac{x'}{\bar{c}} C_D\left(1 + \frac{x'}{l}\right) - \frac{x'}{l}\right]\theta + \left[\frac{C_{m_{\dot{\alpha}}}}{2} D_c + C_{m_\alpha} - \right. \\ & \left. \frac{x'}{\bar{c}} C_{D_\alpha}\theta_o\left(1 + \frac{x'}{l}\right) + \frac{x'}{l}\frac{C_D}{D_c}\right]\alpha + C_{m_{\delta_e}}\delta_e \\ 2\mu_c D_c\alpha = {} & \left[\left(2\mu_c - \frac{C_{L_q}}{2}\right)D_c + C_D\left(1 + \frac{x'}{l}\right) + \frac{C_D\bar{c}}{l}\frac{1}{D_c}\right]\theta + \\ & \left(-C_{L_\alpha} + C_D\frac{x'}{l}\theta_o - \frac{\bar{c}}{l}\frac{C_D}{D_c}\right)\alpha - C_{L_{\delta_e}}\delta_e \end{aligned}\right\} \quad \text{(A32)}$$

The autopilot component which was applicable to the longitudinal degrees of freedom was the elevator component of the automatic position control and the pitch damper. The equation used to represent these components is

$$\delta_e = K_{\theta'}\Delta\theta' + K_{\dot{\theta}}\dot{\theta} \quad \text{(A33)}$$

The towline angle in the vertical plane $\theta'$ is

$$\theta' = \theta_o\left(1 + \frac{x'}{l}\right) - \frac{z}{l} + \left(\frac{x'}{l} + 1\right)\theta$$

The increment in elevator deflection due to the motions is proportional to the change in this angle due to the motion, or

$$\Delta\theta' = \theta' - \theta_o\left(1 + \frac{x'}{l}\right)$$

Therefore,

$$\Delta\theta' = -\frac{z}{l} + \left(\frac{x'}{l} + 1\right)\theta \tag{A34}$$

and the autopilot-component equation becomes

$$\delta_e = K_{\theta'}\left(\frac{x'}{l} + 1\right)\theta - K_{\theta'}\frac{z}{l} + K_{\dot{\theta}}\dot{\theta}$$

In operator form, then

$$\delta_e = K_{\theta'}\left(\frac{x'}{l} + 1\right)\theta + K_{\theta'}\frac{\bar{c}}{l}\frac{(\theta - \alpha)}{D_c} + K_{\dot{\theta}}\frac{V}{\bar{c}}D_c\theta \tag{A35}$$

It can be seen that the use of this autopilot-component equation does not alter the form of the fourth-order characteristic equation.

## REFERENCES

1. Martina, Albert P., and Young, George E.: Results of Initial Wind-Tunnel Flutter Experiments at Low Speed With a Towed Airplane Model Having a 40° Sweptback Wing of Aspect Ratio 3.62 Equipped With Pylon-Mounted Stores. NACA RM L54K17, 1955.

2. Maggin, Bernard, and Shanks, Robert E.: Experimental Determination of the Lateral Stability of a Glider Towed by a Single Towline and Correlation With an Approximate Theory. NACA RM L8H23, 1948.

3. Gardiner, Robert A., and Zarovsky, Jacob: Rocket-Powered Flight Test of a Roll-Stabilized Supersonic Missile Configuration. NACA RM L9K01a, 1950.

4. Schade, Robert O., and Hassell, James L., Jr.: The Effects on Dynamic Lateral Stability and Control of Large Artificial Variations in the Rotary Stability Derivatives. NACA Rep. 1151, 1953. (Supersedes NACA TN 2781.)

5. Weil, Joseph, Sleeman, William C., Jr., and Byrnes, Andrew L., Jr.: Investigation of the Effects of Wing and Tail Modifications on the Low-Speed Stability Characteristics of a Model Having a Thin 40° Swept Wing of Aspect Ratio 3.5. NACA RM L53C09, 1953.

6. Campbell, John P., and McKinney, Marion O.: Summary of Methods for Calculating Dynamic Lateral Stability and Response and for Estimating Lateral Stability Derivatives. NACA Rep. 1098, 1952. (Supersedes NACA TN 2409.)

7. Fisher, Lewis R.: Approximate Corrections for the Effects of Compressibility on the Subsonic Stability Derivatives of Swept Wings. NACA TN 1854, 1949.

8. Jones, B. Melvill: Dynamics of the Aeroplane. Symmetric or Pitching Moments. Vol. V of Aerodynamic Theory, div. N, ch. II, secs. 37-44, W. F. Durand, ed., Julius Springer (Berlin), 1935, pp. 48-54.

TABLE I

MODEL CHARACTERISTICS

| | |
|---|---|
| Weight (model + tanks), lb | 94.2 |
| Moments of inertia: | |
| $I_{X_o}$, slug-ft$^2$ | 3.774 |
| $I_{Y_o}$, slug-ft$^2$ | 6.375 |
| $I_{Z_o}$, slug-ft$^2$ | 8.160 |
| $\eta_o$, deg | 1 |
| Center-of-gravity location measured from nose, ft (21 percent M.A.C.) | 2.97 |
| Wing: | |
| Aspect ratio | 3.45 |
| Sweepback of quarter-chord line, deg | 40 |
| Taper ratio | 0.578 |
| Area, sq ft | 9.02 |
| Span, ft | 5.587 |
| Mean aerodynamic chord, ft | 1.673 |
| Airfoil section (normal to c/4) | NACA 64A010 |
| Wing incidence, deg | 1.5 |
| Dihedral, deg | -3.5 |
| Wing twist, deg | 0 |
| Horizontal tail: | |
| Aspect ratio | 3.59 |
| Sweepback of the quarter-chord line, deg | 40 |
| Taper ratio | 1.0 |
| Area, sq ft | 1.55 |
| Span, ft | 2.362 |
| Chord, ft | 0.667 |
| Airfoil section normal to quarter-chord line | NACA 64A009 |
| Twist, deg | 0 |
| Dihedral, deg | 0 |
| Tail length, ft | 3.267 |
| Elevator: | |
| Hinge line, percent of stabilizer chord | 70 |
| Chord, ft | 0.200 |
| Inboard elevator span, ft | 0.518 |
| Outboard elevator span, ft | 0.518 |
| Elevator area (total), sq ft | 0.207 |
| Vertical stabilizer: | |
| Aspect ratio | 1.45 |
| Sweepback of quarter-chord line, deg | 41.3 |
| Taper ratio | 0.467 |
| Area, sq ft | 1.215 |
| Span, ft | 1.263 |
| Mean aerodynamic chord, ft | 0.927 |
| Airfoil section normal to quarter-chord line | NACA 64A011 |
| Tail length, ft | 2.928 |
| Rudder: | |
| Chord (parallel to fuselage center line), ft | 0.228 |
| Span, upper segment, ft | 0.556 |
| Span, lower segment, ft | 0.556 |
| Aileron: | |
| Hinge line, percent of wing chord perpendicular to quarter-chord line | 75 |
| Aileron chord inboard (parallel to center line), ft | 0.430 |
| Aileron chord outboard (parallel to center line), ft | 0.360 |
| Span (15.5 percent to 52 percent b/2), ft | 1.103 |
| Fuselage: | |
| Length, ft | 6.403 |
| Frontal area, sq ft | 0.5397 |
| Fineness ratio | 7.75 |

TABLE II

AUTOPILOT CHARACTERISTICS

| | |
|---|---|
| **Roll Autopilot:** | |
| Weight (total including relays), lb | 10 |
| **Gyro:** | |
| Voltage, d-c | 24 to 26 |
| Speed, rpm | 13,500 |
| **Torque motor:** | |
| Voltage, d-c | 24 to 26 |
| Stalling torque, in-lb | 2.98 |
| Stalling current, amp | 15.7 |
| Gearing (motor to cam) | 44.8:1 |
| **Cam:** | |
| Angle, deg | 28 |
| Efficiency (approx.), percent | 75 |
| Gearing (output arm to gimbal) | 0.333:1 |
| **Trim coil:** | |
| Voltage, d-c | 24 to 26 |
| Current at 24 V d-c, ma | 290 |
| Torque on inner gimbal, in-oz | 7 |
| Precession rate of outer gimbal (gyro speed, 11,700 rpm) (no load), deg/sec | 1.3 |
| **Damper Autopilot:** | |
| **Rotor:** | |
| Speed, rpm - | |
| At 1 lb/sq in. | 10,000 |
| At 7 lb/sq in. | 90,000 |
| Natural frequency, cps - | |
| At 85,200 rpm | 60 |
| At 20,000 rpm | 155 |
| Percent critical damping - | |
| At 85,200 rpm | 0.09 |
| At 20,000 rpm | 0.21 |
| **Pickoff (flapper-venturi nozzles):** | |
| Spacing | 0.010" to 0.011" plus flapper |
| Pressure, lb/sq in. | 7 to 8 |
| **Servo (ACS miniature pneumatic):** | |
| Stroke, in. | ±1/4 |
| Piston area, sq in. - | |
| Front | 0.6012 |
| Rear | 0.574 |
| Feedback spring (8.5 turns of 0.026 in. music wire), in. O.D. | 0.542 |
| Force output at 20 lb/sq in., lb | 8 |
| Natural frequency, radians/sec | 40 to 25 |
| Damping | 0.6 to 0.8 |

TABLE III

AERODYNAMIC COEFFICIENTS

| | | |
|---|---|---|
| V, mph | 100 | 200 |
| $C_L$ | 0.417 | 0.104 |
| $C_D$ | 0.045 | 0.023 |
| $C_{l_\alpha}$ | 3.553 | 3.610 |
| $C_{D_\alpha}$ | 0.264 | 0.066 |
| $C_{m_\alpha}$ | -0.659 | -0.688 |
| $C_{Y_\beta}$ | -0.741 | -0.701 |
| $C_{n_\beta}$ | 0.218 | 0.197 |
| $C_{l_\beta}$ | -0.095 | -0.092 |
| $C_{Y_r}$ | 0.551 | 0.582 |
| $C_{n_r}$ | -0.335 | -0.332 |
| $C_{l_r}$ | 0.119 | 0.107 |
| $C_{Y_p}$ | 0.330 | 0.111 |
| $C_{n_p}$ | -0.064 | -0.026 |
| $C_{l_p}$ | -0.209 | -0.294 |
| $C_{m_q}$ | -4.492 | -4.584 |
| $C_{m_{\dot{\alpha}}}$ | -2.315 | -1.689 |
| $C_{l_{\delta_a}}$ | 0.060 | 0.060 |
| $C_{n_{\delta_a}}$ | -0.024 | -0.024 |
| $C_{l_{\delta_r}}$ | 0.006 | 0.006 |
| $C_{n_{\delta_r}}$ | -0.060 | -0.060 |
| $C_{Y_{\delta_r}}$ | 0.030 | 0.030 |
| $C_{m_{\delta_\epsilon}}$ | -0.355 | -0.349 |
| $C_{l_{\delta_\epsilon}}$ | 0.339 | 0.168 |

TABLE IV

COMPARISON OF EXPERIMENTAL AND CALCULATED PERIODS OF MOTION

[All periods are in seconds; velocity is in feet per second]

| Wing | V | $K_{\psi'}$ | $K_{\phi}$ | $K_{\dot{\psi}}$ | $K_{\theta}$ | $K_{\dot{\theta}}$ | Lateral Motion | | | | | | Longitudinal Motion | | | |
|---|---|---|---|---|---|---|---|---|---|---|---|---|---|---|---|---|
| | | | | | | | Short | | Middle | | Long | | Short | | Long | |
| | | | | | | | $P_{exp.}$ | $P_{calc.}$ | $P_{exp.}$ | $P_{calc.}$ | $P_{exp.}$ | $P_{calc.}$ | $P_{exp.}$ | $P_{calc.}$ | $P_{exp.}$ | $P_{calc.}$ |
| Rigid | 145 | 1 | 4.0 | 0.48 | 2.6 | 0 | 0.59 | 0.73 | 0.98 | 1.15 | 6.42 | 8.67 | 0.60 | 0.58 | 2.25 | 2.16 |
| Rigid | 296 | .50 | 3.5 | .30 | 2.2 | .60 | .47 | .45 | 1.55 | 1.09 | 4.30 | 4.82 | .46 | .23 | 1.62 | 1.54 |
| Flexible | 162 | 1 | 5.2 | .54 | 2.0 | .50 | .55 | ---- | 1.10 | ---- | 5.82 | ---- | .92 | ---- | 2.10 | ---- |
| Flexible | 280 | .50 | 4.0 | .39 | 2.0 | .50 | .59 | ---- | ---- | ---- | 2.74 | ---- | .51 | ---- | 1.95 | ---- |
| Rigid | 145 | .75 | 5.6 | .50 | --- | ---- | .72 | .59 | 1.13 | 1.10 | 5.70 | 9.45 | ---- | ---- | ---- | ---- |
| Rigid | 145 | .75 | 4.0 | .50 | --- | ---- | .69 | .68 | 1.04 | 1.11 | 7.40 | 9.23 | ---- | ---- | ---- | ---- |

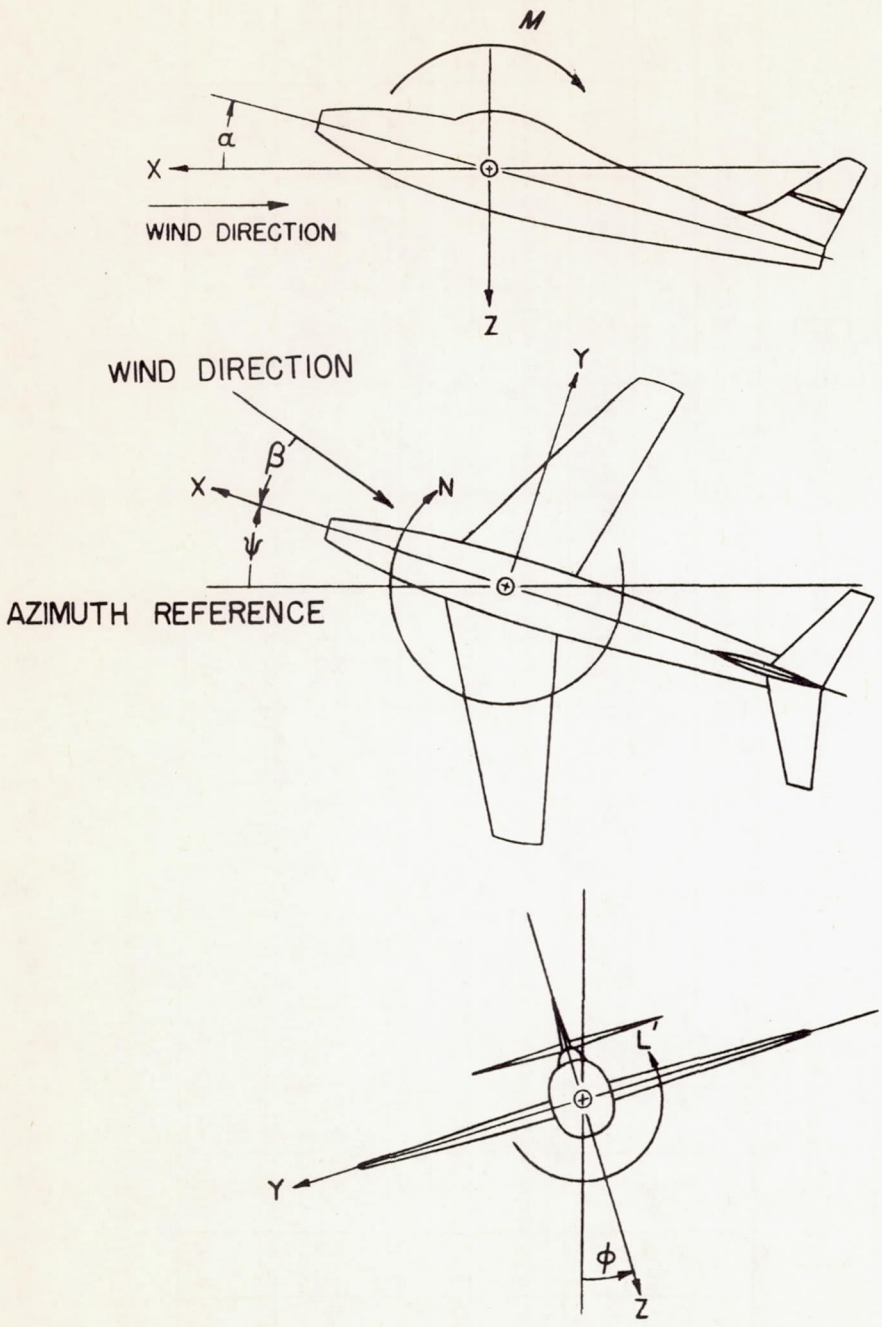


Figure 1.- The stability system of axes. Arrows indicate positive directions of moments, forces, and angles. This system of axes is defined as an orthogonal system having the origin at the center of gravity and in which the Z-axis is in the plane of symmetry and perpendicular to the relative wind in the undisturbed flight condition, the X-axis is in the plane of symmetry and perpendicular to the Z-axis, and the Y-axis is perpendicular to the plane of symmetry. During disturbed flight, the axes remain fixed in the airplane.

| | |
|---|---|
| Wing area | 9.02 $ft^2$ |
| Taper ratio | 0.578 |
| Mean aerodynamic chord | 20.08 in. |
| Aspect ratio | 3.45 |

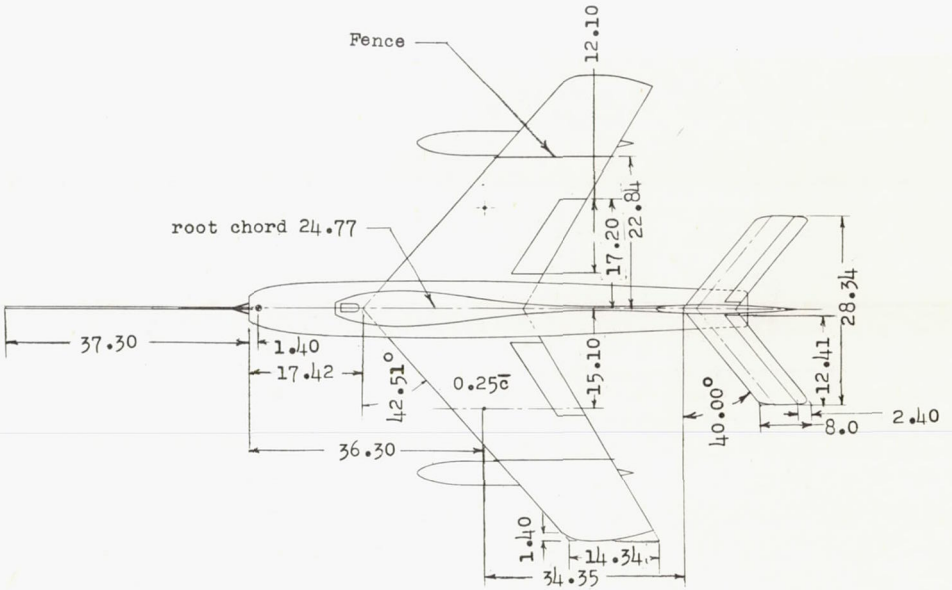


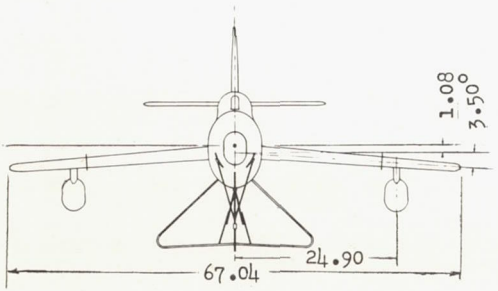


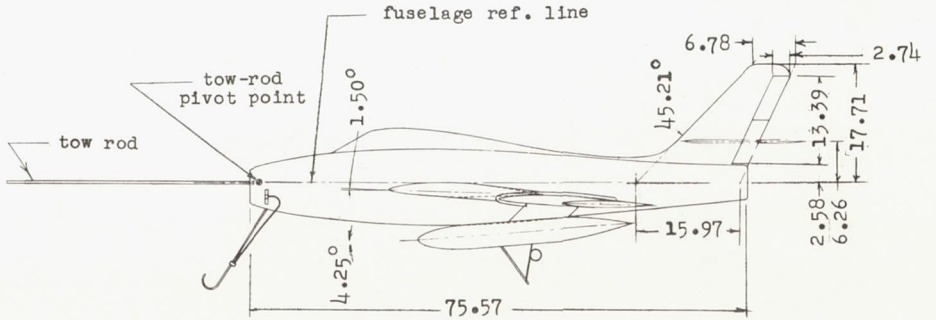


Figure 2.- Principal dimensions of the model. All dimensions in inches unless otherwise noted.

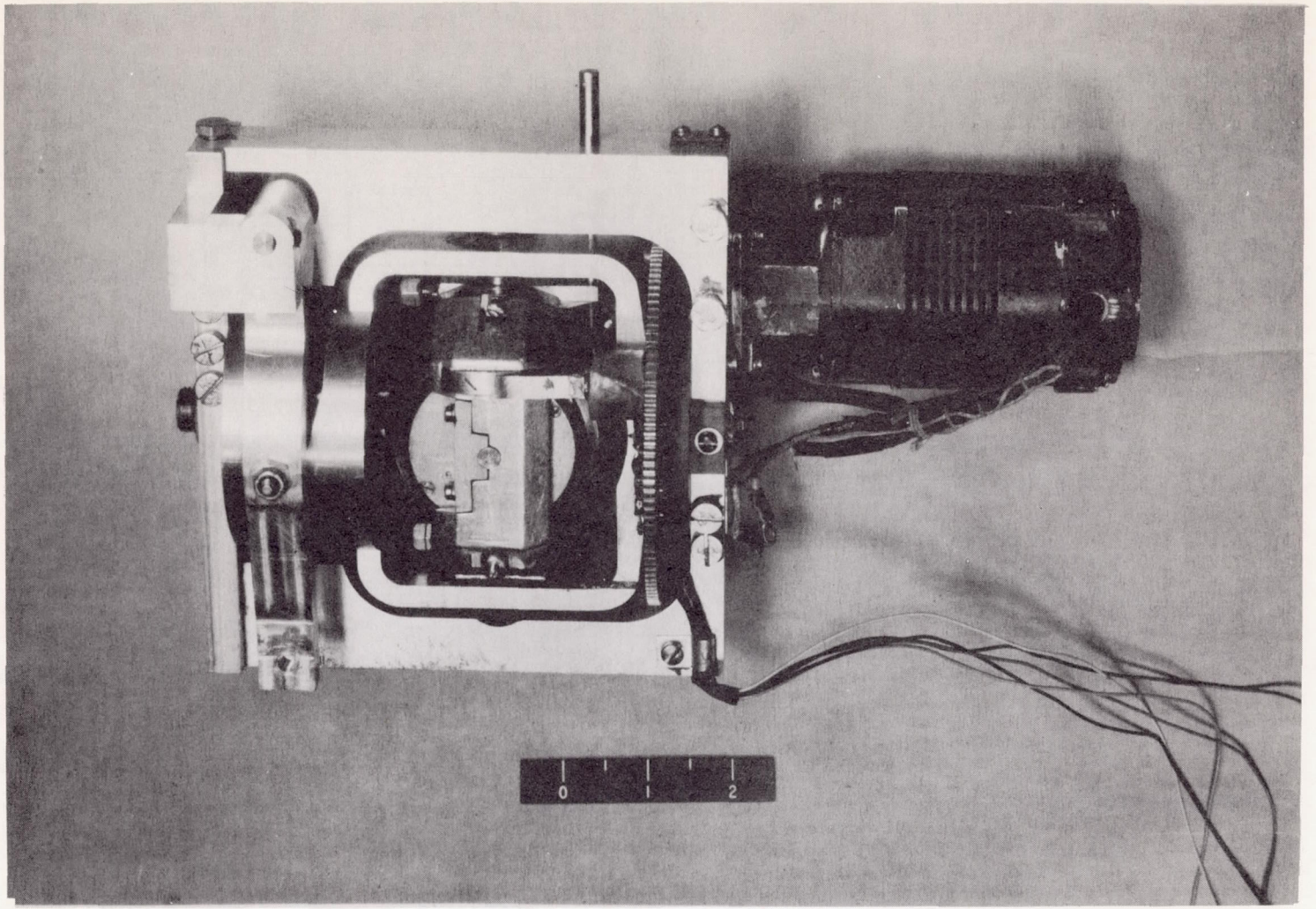


L-78758

Figure 3.- Photograph of the roll-control autopilot component used in the towed model.

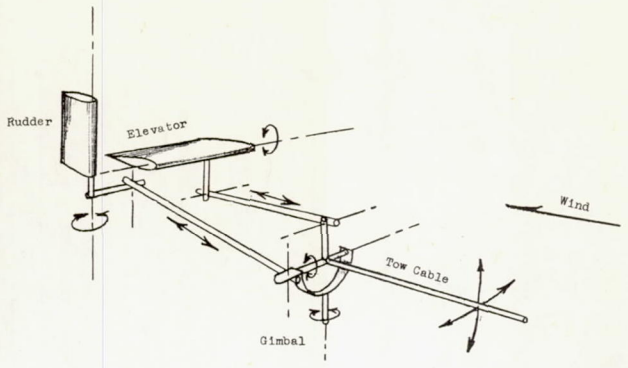


Automatic Position Control

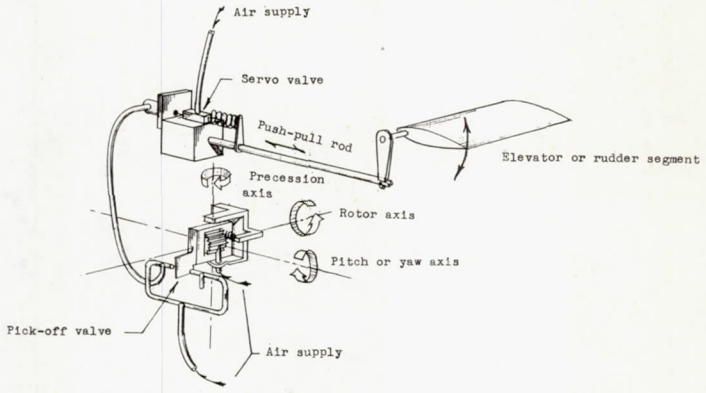


Pitch or Yaw Damper

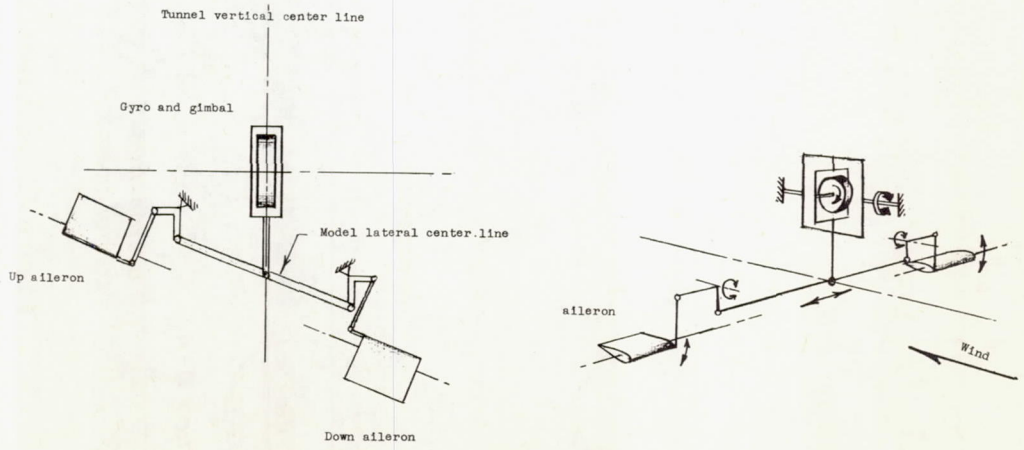


Roll Control

Figure 4.- Schematic representations of the components of the autopilot system used in the towed model.

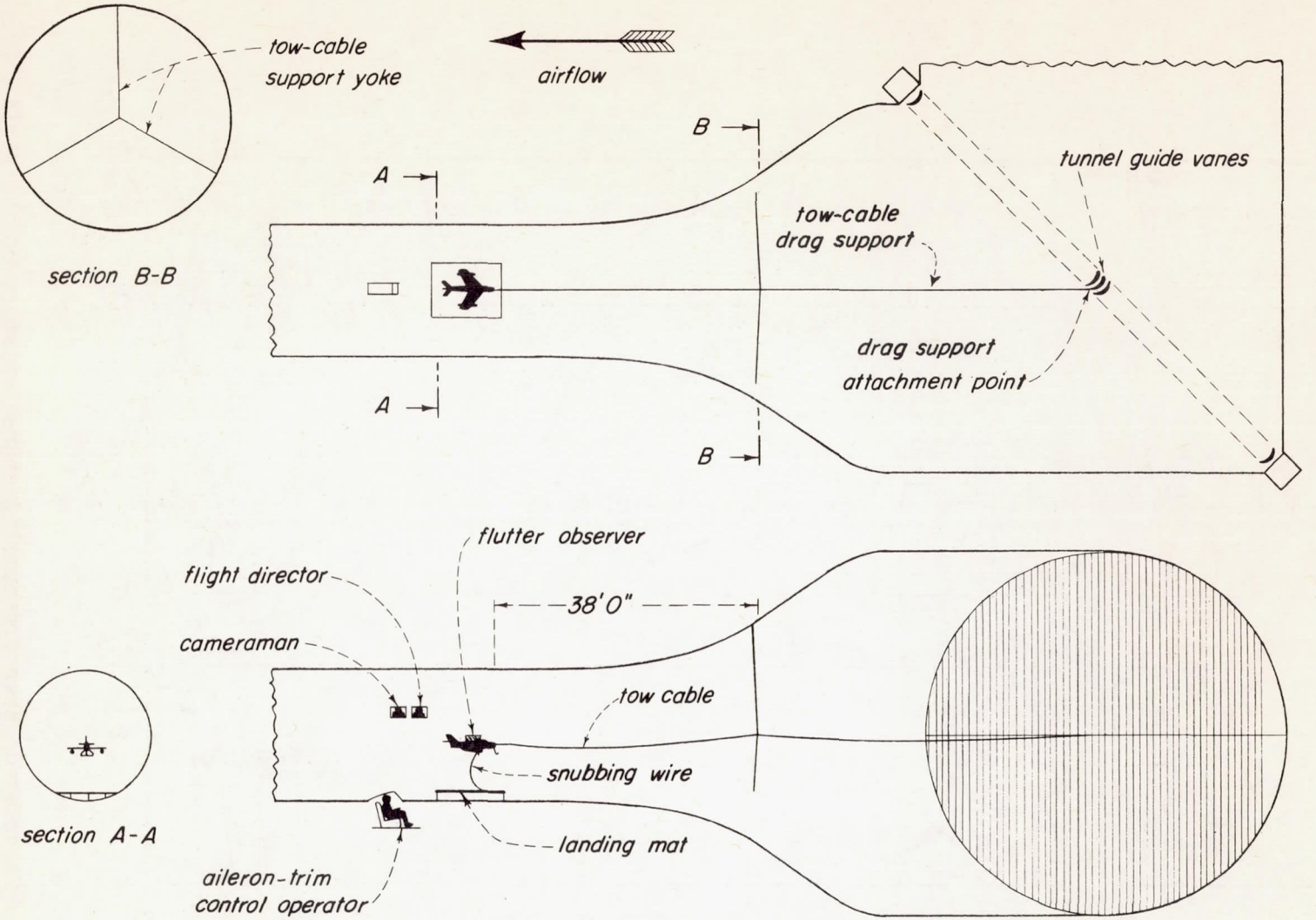


Figure 5.- Schematic representation of test arrangement in the Langley 19-foot pressure tunnel for the towed model tests.

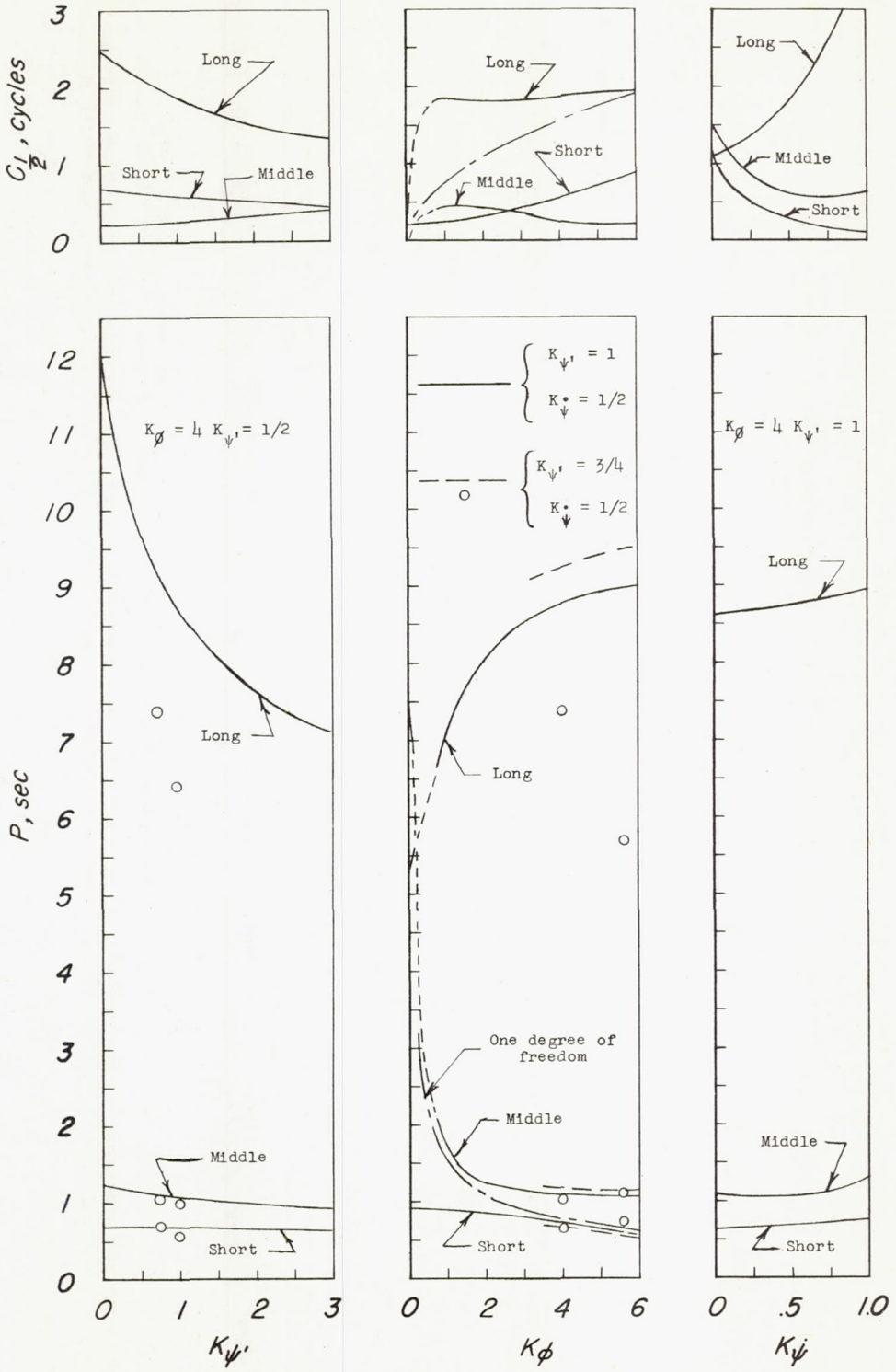


Figure 6.- Calculated lateral stability characteristics of the rigid wing model at V = 145 ft/sec, with varying autopilot gearing ratios. Symbols denote experimental periods.

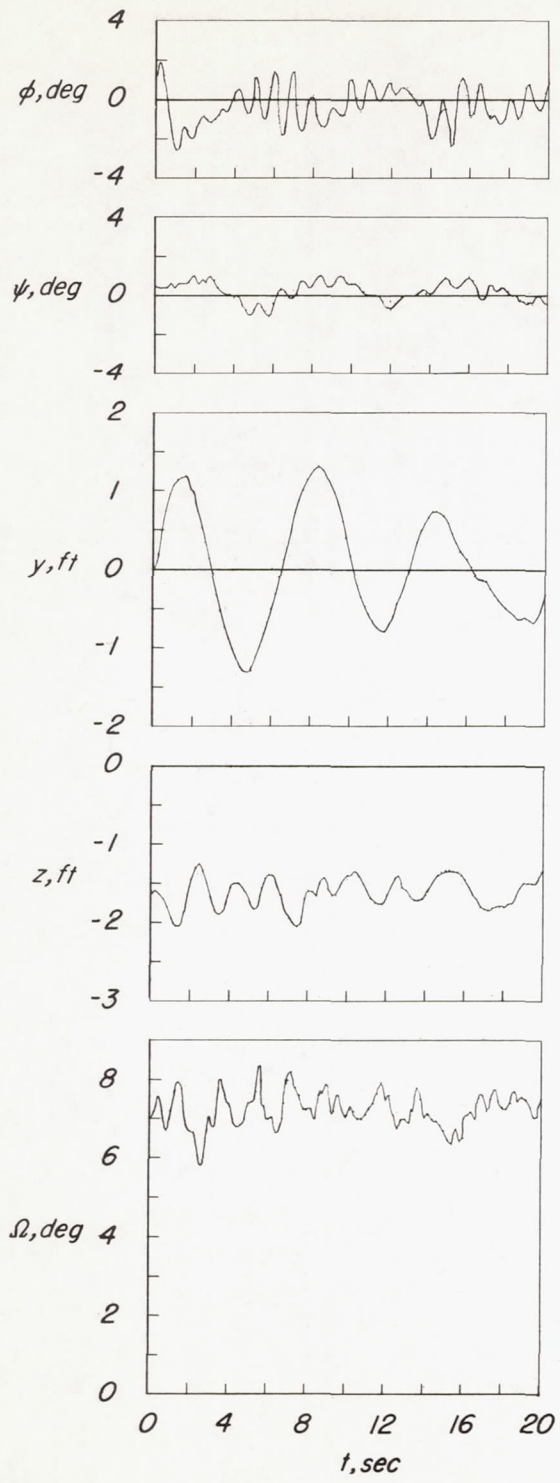


(a) V = 145 ft/sec; $K_{\psi}' = 1$; $K_{\phi} = 4.0$; $K_{\dot{\psi}} = 0.48$; $K_{\theta}' = 2.6$; $K_{\dot{\theta}} = 0$.

Figure 7.- Experimental time history of the rigid wing model.

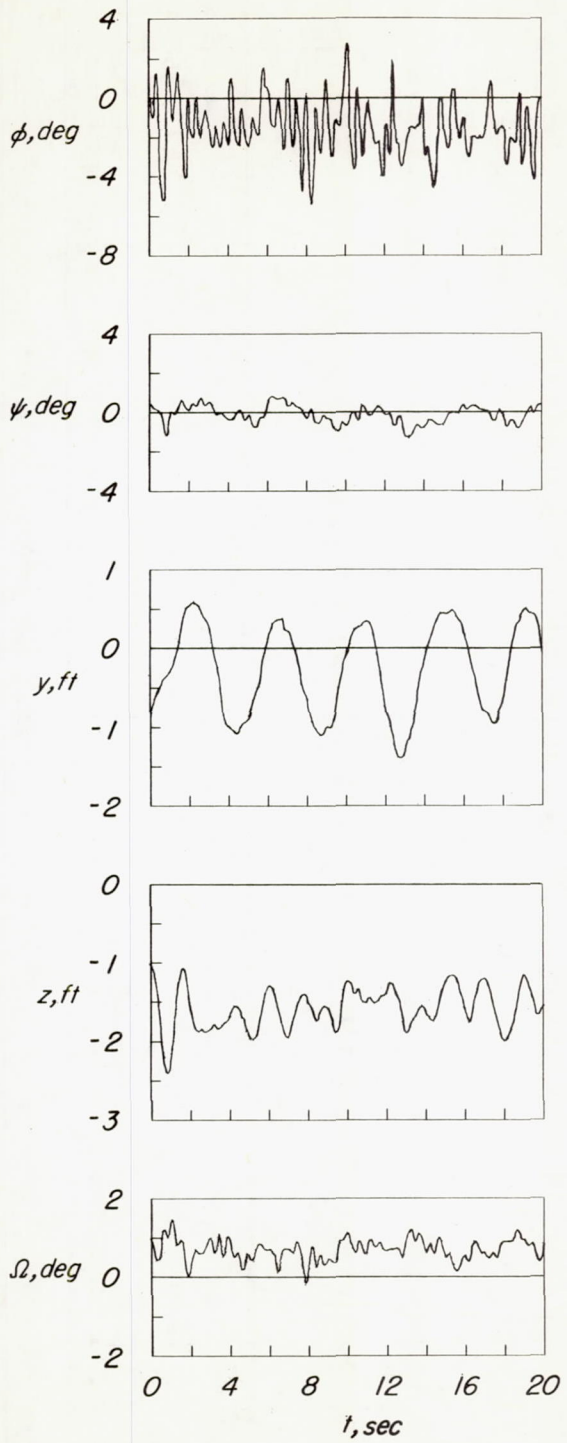


(b) V = 296 ft/sec; $K_{\psi'} = 0.50$; $K_{\phi} = 3.5$; $K_{\dot{\psi}} = 0.30$; $K_{\theta'} = 2.2$; $K_{\dot{\theta}} = 0.60$.

Figure 7.- Concluded.

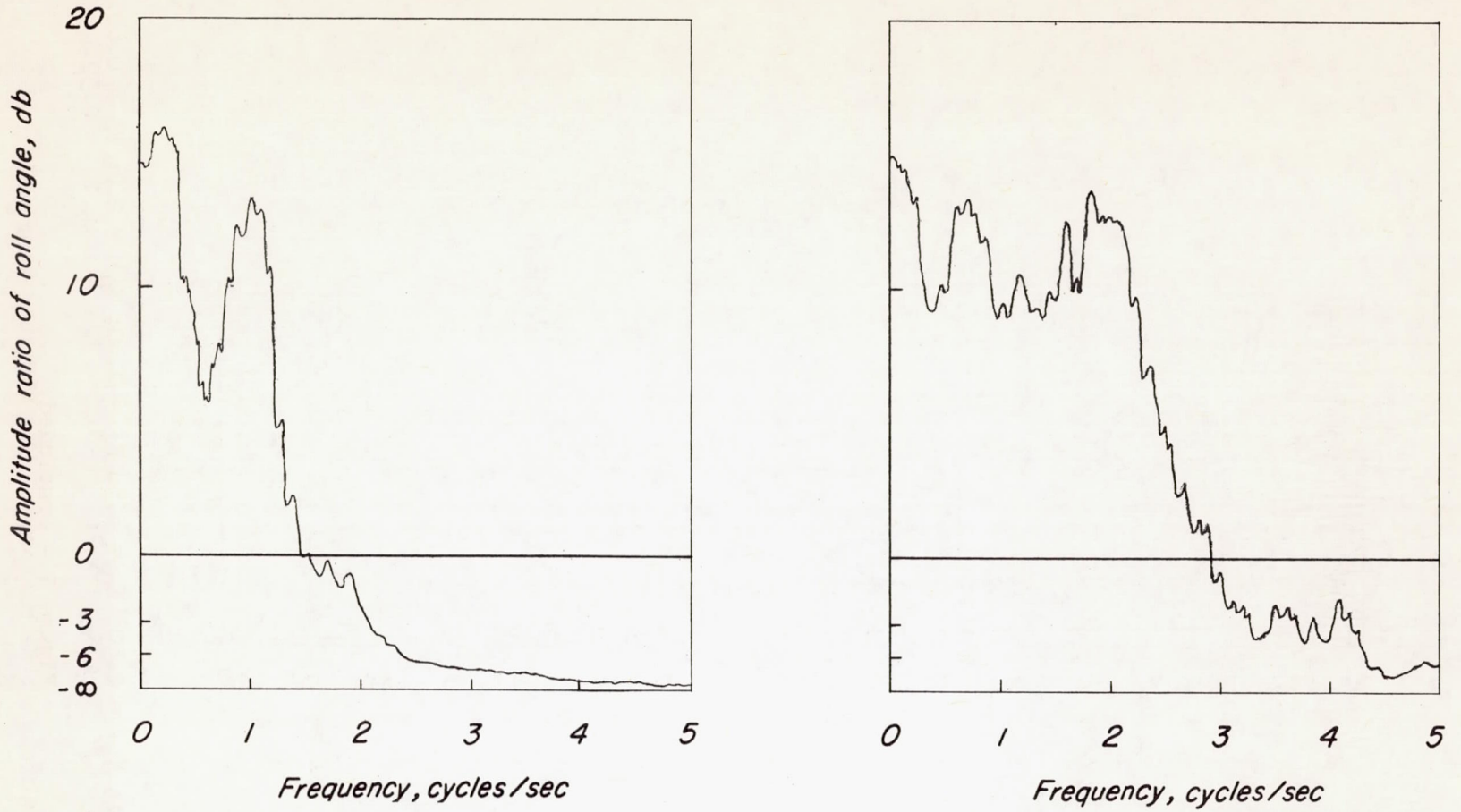


(a) V = 145 ft/sec; $K_{\psi}'$ = 1.0; $K_{\phi}$ = 4.0; $K_{\dot{\psi}}$ = 0.48; $K_{\theta}'$ = 2.6; $K_{\dot{\theta}}$ = 0.

(b) V = 296 ft/sec; $K_{\psi}'$ = 0.5; $K_{\phi}$ = 3.5; $K_{\dot{\psi}}$ = 0.30; $K_{\theta}'$ = 2.2; $K_{\dot{\theta}}$ = 0.60.

Figure 8.- Typical power-spectrum-density analyses of the angle of roll $\phi$ of the rigid wing model.

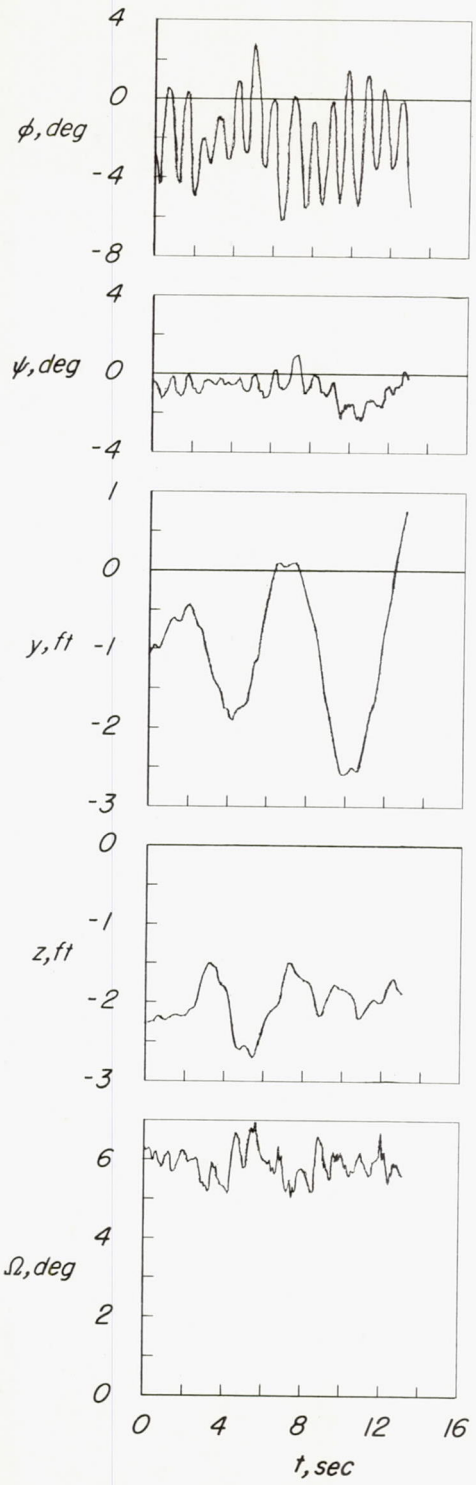


(a) V = 162 ft/sec; $K_{\psi}' = 1$; $K_{\phi} = 5.2$; $K_{\dot{\psi}} = 0.54$; $K_{\theta}' = 2.0$; $K_{\dot{\theta}} = 0.50$.

Figure 9.- Experimental time history of the flexible wing model.

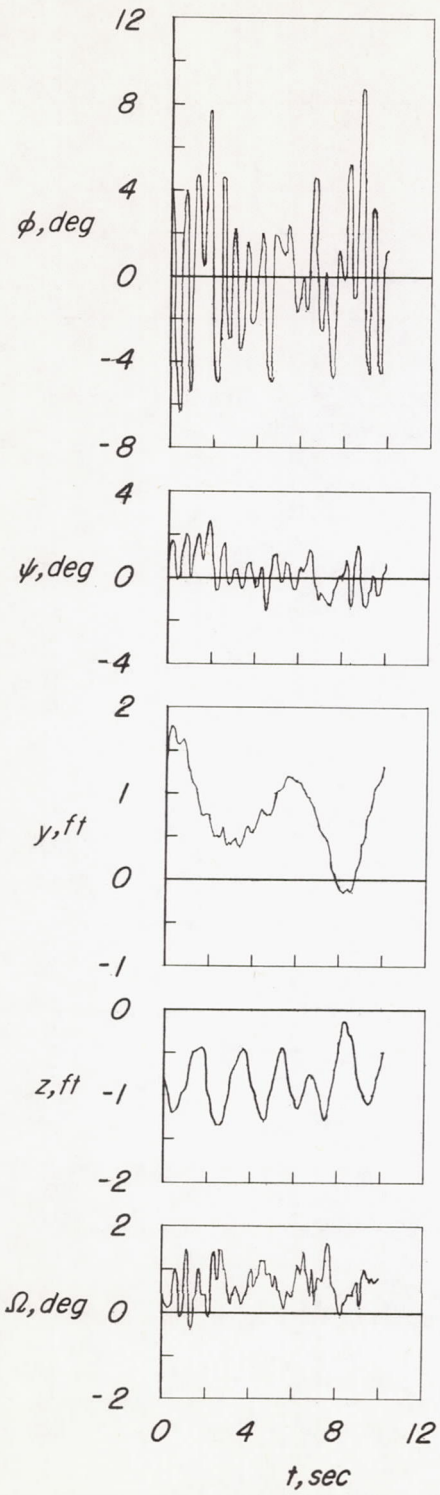


(b) V = 280 ft/sec; $K_{\psi'} = 0.50$; $K_{\phi} = 4.0$; $K_{\dot{\psi}} = 0.39$; $K_{\theta'} = 2.0$; $K_{\dot{\theta}} = 0.50$.

Figure 9.- Concluded.

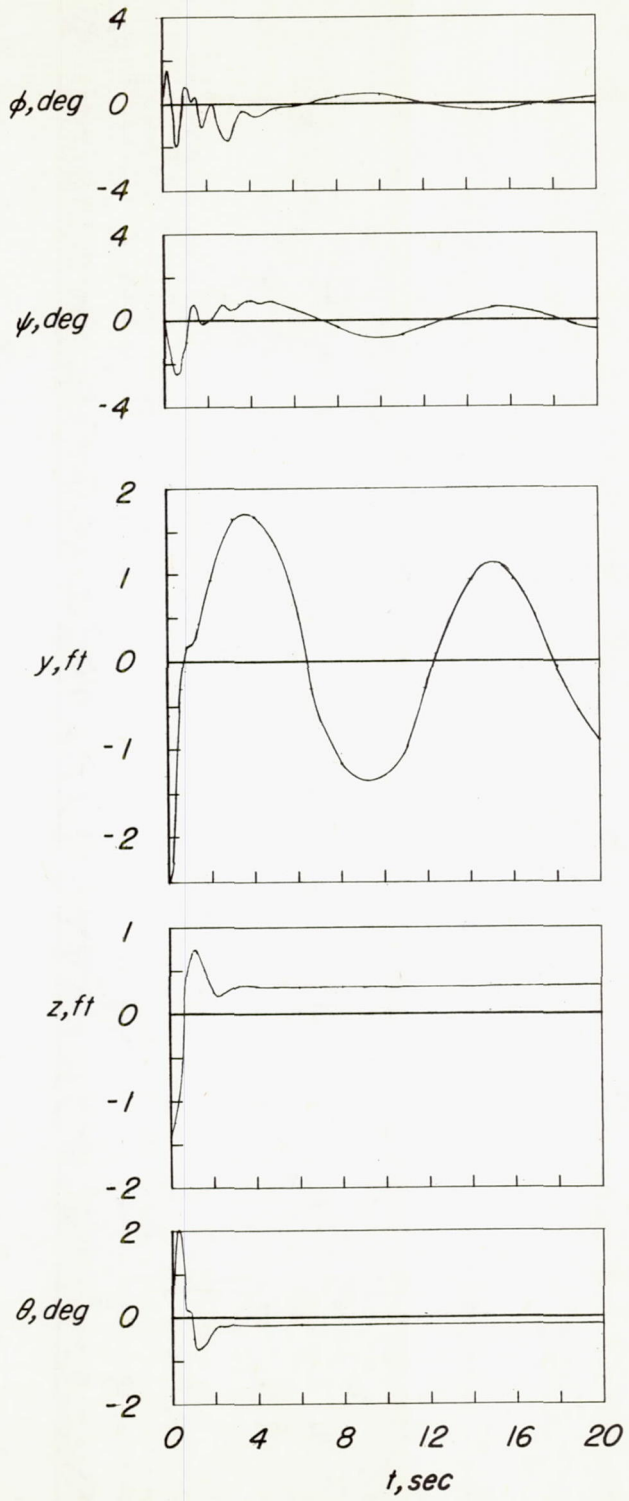


(a) V = 146 ft/sec; $K_{\psi}' = 1$; $K_{\phi} = 4.0$; $K_{\dot{\psi}} = 0.48$; $K_{\theta}' = 2.6$; $K_{\dot{\theta}} = 0$.

Figure 10.- Calculated time history of the rigid wing model.

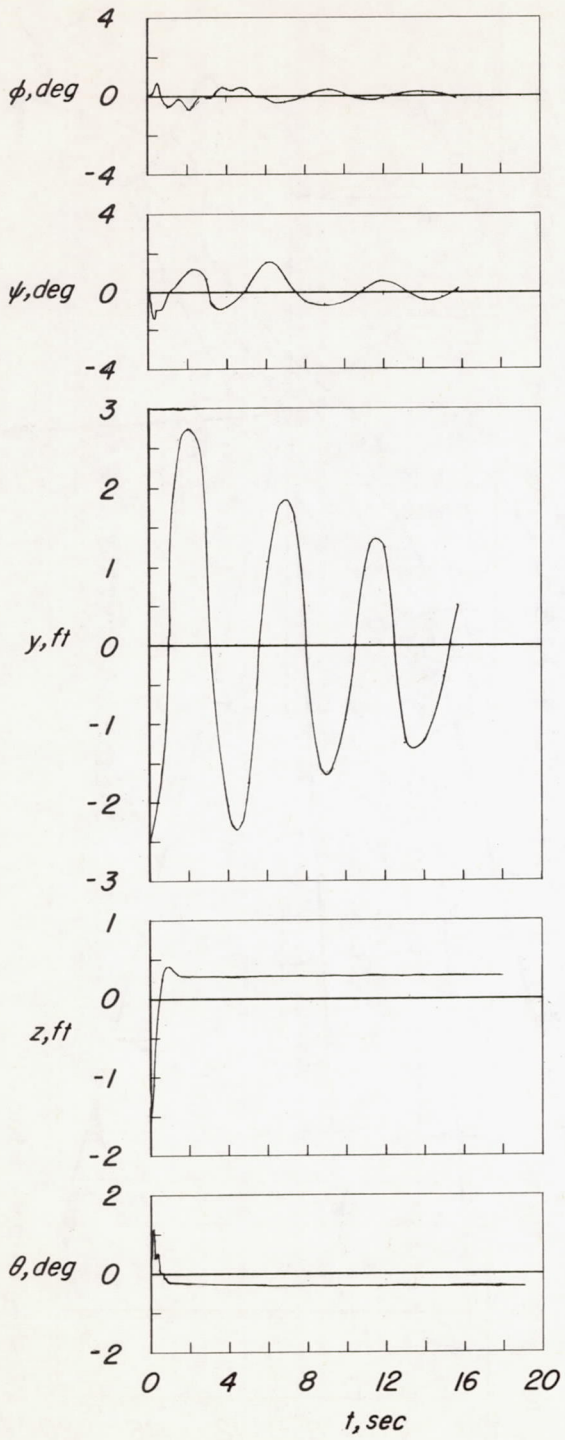


(b) V = 293 ft/sec; $K_{\psi}' = 0.50$; $K_{\phi} = 3.5$; $K_{\dot{\psi}} = 0.30$; $K_{\theta}' = 2.2$; $K_{\dot{\theta}} = 0.60$.

Figure 10.- Concluded.

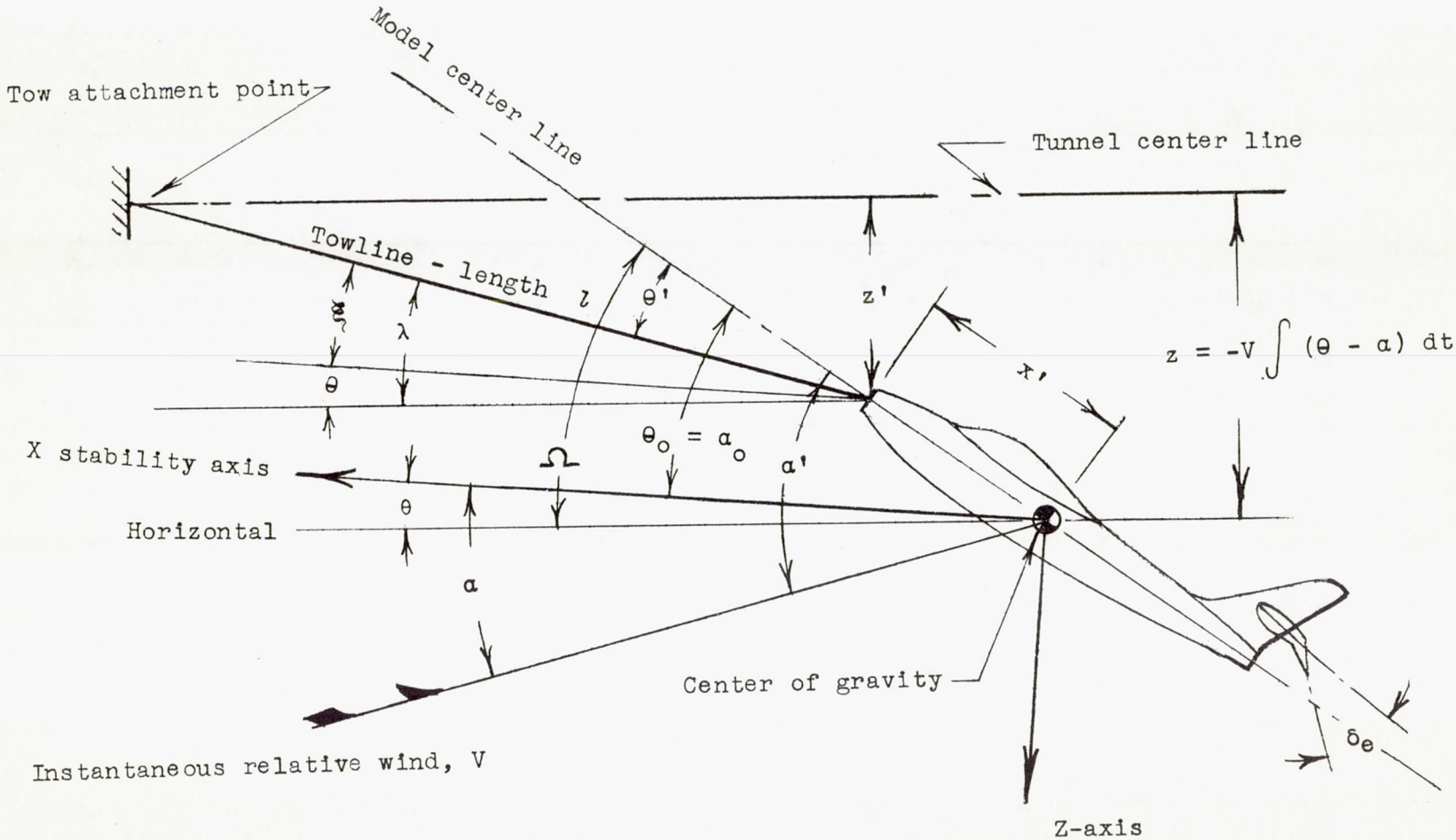


Figure 11.- Schematic representation of the model. Towline combination used in developing the longitudinal equations of motion.



NACA-Langley - 3-25-55 - 32